JNC TN9400 2000-022

Passive Electromagnetic NDE for Mechanical Damage Inspection by Detecting Leakage Magnetic Flux

Ⅱ An Experimental Study on the Correlation of Natural Magnetization and Mechanical Damages in the SUS304 Stainless Steel

March 2000

O-ARAI ENGINEERING CENTER

JAPAN NUCLEAR CYCLE DEVELOPMENT INSTITUTE

本資料の全部または一部を複写・複製・転載する場合は，下記にお問い合わせください。

〒319-1184　茨城県那珂郡東海村村松４番地49
核燃料サイクル開発機構
技術展開部　技術協力課

Inquiries about copyright and reproduction should be addressed to :
Technical Cooperation Section,
Technology Management Division,
Japan Nuclear Cycle Development Institute
4-49 Muramatsu, Tokai-mura, Naka-gun, Ibaraki 319-1184, Japan.

© 核燃料サイクル開発機構 (Japan Nuclear Cycle Development Institute)
2000

JNC TN9400 2000 – 022
March, 2000

Passive Electromagnetic NDE for Mechanical Damage Inspection by Detecting Leakage Magnetic Flux

II An Experimental Study on the Correlation of Natural Magnetization and Mechanical Damages in the SUS304 Stainless Steel

Zhenmao CHEN, Kazumi AOTO, Syoichi KATO and Yuji NAGAE*

Abstract

In this report, a study on the behaviors of the magnetization induced by mechanical damages is carried out. By introducing mechanical damages to a test-piece with a tension or/and a zero-tension fatigue testing and measuring the corresponding leakage flux signal, natural magnetization change is proved and found increasing with the mechanical damages (viz. plastic deformation or fatigue damages) though a saturation occurs when damage gets too large. From the experimental results of fatigue testing utilizing test-pieces with a central slit, it was verified that observing the natural leakage flux density (leakage flux without applying external magnetic field) is a reasonable way to identify fatigue cracks. A feature parameter (area of the $\varepsilon \sim B$ hysteresis curve) of the in-situ magnetic field signal measured during the fatigue testing is proposed for predicting the fatigue damages, which is found depending on the cyclic number of the applied loading. At last, residual magnetic fields of a magnetized test-piece are also measured and found depending on the applied plastic deformation in case that the plastic strain is not too small. From these experimental results, it is found that the approach detecting natural magnetization is applicable for monitoring the damage status though it may be not efficient for a scanning inspection concerning its small signal magnitude. On the other hand, the method employing permanent magnet is robust against the environment noise but possibly not valid for the ISI of a structural component with a relative low damage level. For practical application, efforts to evaluate the feasibility of the proposed method are necessary for more testing conditions especially its suitability in a practical environment.

---

* Structure Safety Engineering Group, OEC/JNC

JNC TN9400 2000 − 022
２０００年　３月

自然磁束漏洩の計測による材料損傷の非破壊評価に関する研究
(第２報 SUS304 ステンレス鋼における自然磁化と損傷の相関に関する試験)

(研究報告)

陳 振茂, 青砥 紀身, 加藤 章一, 永江 勇二 *

概要

本研究では SUS304 ステンレス鋼における自然磁化と機械損傷の相関に関する試験研究を実施した。単純引張試験及び両振疲労試験を用いて試験片に機械損傷を与え、フラクスゲートセンサーで試験中及び除荷後の磁化特性を測定した。その結果外部磁場をかけなくても塑性変形や疲労損傷により自然磁化が発生し、損傷の増加と伴い飽和することが明らかにした。切欠試験片に疲労き裂を入れた試験から、自然磁化は特に疲労き裂の検査に有効であることが判った。更に疲労試験中測定した磁場信号の処理により、疲労損傷の検出に適用可能な信号の特徴量 (磁場・ひずみヒシテリシス曲線の面積) を提案した。最後に塑性変形を与えた試験片に対して永久磁石励磁による残留磁化の分布を測定し、残留磁化は塑性変形が十分大きくなると増加する傾向があると判った。上記内容から、損傷誘起自然磁化は絶対値が小さいものの、特徴量の抽出やセンサーの工夫によって損傷状態の監視に十分適用可能であると考えられる。一方、自然磁化の測定は走査検査への適用のためにまた努力する必要があるが、これに対して残留磁化に基づいた手法は有効である可能性が高い。なお、提案手法を実機環境への応用に至るまでは、異なる試験条件下の挙動や実環境ノイズの影響の確認などさらなる研究を重ねる必要があると考えられる。

* 大洗工学センター、Na 安全工学試験部、機器・構造安全工学グループ

Contents

Abstract i

List of Tables v

List of Figures vii

1. Introduction 1

2. Experimental Issues 3
2.1 Test material and test-pieces 3
2.2 Measuring Method and Experimental Set-ups 3
2.3 Experimental Procedure 6

3. Experimental Results 8
3.1 Results of the tensile testing 8
3.2 Results of the Fatigue Testing 10
3.3 Results in case with a magnetizing procedure 13

4. Discussions 15
4.1 The principle of the natural magnetization 15
4.2 The correlation of the magnetization and the plastic strain 16
4.3 Correlation of the fatigue damages and the feature parameters of the detected magnetic field signals 16
4.4 The possibility to detect plastic damages from magnetic parameters of the SUS304 steel 17
4.5 The possibility to detect damage by using the natural magnetization . . 18

5. Conclusions and Prospect Work 19

6. Acknowledgments 20

References 21

List of Tables

Table 1 Composition of the SUS304 A3 material 3

Table 2 Measured testpieces and their test conditions 7

Table 3 Comparison of the number of the slipped grains 9

Table 4 Comparison of the strains measured by moire method and strain sensor 10

Table 5 Comparison of the proportional limits and the changes of the magnetic field .. 18

List of Figures

Fig.1 Shape of the button type CCT testpiece 22
Fig.2 Principle diagram of the FG sensor 22
Fig.3 Schematic diagrams of the insitu measuring system 23
Fig.4 The measuring system of moiré method 23
Fig.5 Fixing instrument for setting sensors 24
Fig.6 Setting locations of the FG sensors 24
Fig.7 Experimental setup of the off-situ scanning system 25
Fig.8 Setup of the magnetizing system 25
Fig.9 Insitu measuring result of NDT2 during tensile testing (NDT2, 0% ~ 3%) 26
Fig.10 Insitu measuring result during tensile testing (NDT2, 3% ~ 6%) 26
Fig.11 Distribution of the natural magnetic field after tensile testing (NDT2, 0% ~ 3%) 27
Fig.12 Distribution of the natural magnetic field after tensile testing (NDT2, 3% ~ 6%) 27
Fig.13 Insitu measuring result during tensile testing (NDT21, 0% ~ 3%) 28
Fig.14 Location of the samples cut out from testpiece NDT2 28
Fig.15 Comparison of the microstructure of the samples cut out from different positions (NDT2, after 9% tension) 29
Fig.16 Comparison of the local slipping of the sample at the top and bottom side of the testpiece NDT2 (after 9% tension) 30
Fig.17 TEM image of sample cut from the bottom side of the tesepiece NDT2 (after 9% tension) 31
Fig.18 X-ray diffration images for determining the property of the various phases shown in the Fig.17 31
Fig.19 An example of the fringe patterns of the moire method for testpiece NDT14 unloaded after tensile testing ($\varepsilon \simeq 3.78\%$) 32
Fig.20 Insitu signals for testpiece NDT14 and strain range 0.08% ~ 0.5% 32
Fig.21 Insitu signals for testpiece NDT14 and strain range 0.35% ~ 1.08% 33
Fig.22 Distribution of the flux density fortestpiece NDT21 after fatigue crack was initiated 33
Fig.23 Distribution of the flux density for testpiece NDT20 after fatigue crack was initiated 34
Fig.24 The magnetization image at the crack tip of the testpiece NDT21 obtained by using the colloidal method 34

Fig.25 The observing areas of the MFM 35

Fig.26 An example of the MFM image at the crack region (mechanical polish) 35

Fig.27 An example of the MFM image at the crack region (chemical polish) 36

Fig.28 Comparison of magnetic field signal during the fatigue testing of testpiece NDT14 (with residual strain) and NDT13 (virgin material) 36

Fig.29 Distribution of magnetic field measured after fatigue crack initiated (NDT13, 63000 cycle) 37

Fig.30 Magnetic field signals at different cyclic number for testpiece NDT13 (virgin material) 37

Fig.31 Typical hysteresis curves of the magnetic field versus applied strain 38

Fig.32 Typical hysteresis curves of the magnetic field versus applied loading 39

Fig.33 Distribution of the residual magnetic field B_y after magnetized with a permanent magnet (NDT12, Residual strain: 0.84%) 40

Fig.34 Distribution of the residual magnetic field B_y after magnetized with a permanent magnet (Residual strain: 1.82%) 40

Fig.35 Distribution of the residual magnetic field B_y after magnetized with a permanent magnet (Residual strain: 5.76%) 41

Fig.36 Insitu measuring result for the magnetized testpiece NDT12 (strain range, $0 \sim 0.2\%$) 41

Fig.37 Insitu measuring result for the magnetized testpiece NDT12 (strain range, $0.08\% \sim 0.5\%$) 42

Fig.38 In-situ measuring result for the magnetized testpiece NDT12 (strain range, $0.35\% \sim 1.0\%$) 42

Fig.39 In-situ measuring result for the magnetized testpiece NDT12 (strain range, $0.95\% \sim 2.0\%$) 43

Fig.40 Insitu signale of the magnetic field for testpiece NDT12, which is demagnetized and magnetized after a tension to a strain of 6.0% ($0 \sim 100$ cycle) 43

Fig.41 The decrement of the plastic deformation induced magnetization for testpiece NDT14 and NDT2 44

Fig.42 Evolution of the area of the $B - \varepsilon$ hysteresis curve during fatigue testing of testpiece NDT13 44

Fig.43 Evolution of the area of the $B - \varepsilon$ hysteresis curve during fatigue testing for testpiece NDT13 and sensor 1 45

Fig.44 Correlation of the cyclic number and the amplitude of the measured natural magnetic field 45

Fig.45 Correlation of the residual magnetic field and the applied plastic strain 46

Fig.46 The concept diagram for the definition of the ε_p, ε_{py} and B_y^{max} 46

1. Introduction

Nowadays, for enhancing the safety of various critical structure systems such as the machinery of a nuclear power plant, more reliable NonDestructice Evaluations (NDE) are strongly expected by the related industry society. In addition, the improvement of the inspection efficiency is also a challenging subject as it is getting more important for dealing with the costdown issue, which, as well known, may affect the future of the related industries. An example of such needs is an efficient technique for predicting the initiation of fatigue cracks, or in other word, to evaluate the status of damages or degradations in an aged structure component for preventing severe failure. It is easy to understand that such a technique also relates with a huge economic benefit in view of the enhancement of the efficiency and reliability of the maintenance technique.

Recently, it was found that a magnetization occurs in the vicinity of a fatigue crack even in an environment without any external magnetic field (excepting the field of the earth) for the austenitic stainless steel of SUS304 type and some other normal carbon steels[1],[2]. The reason of such a phenomenon is considered as an effect of the magnetic property alternating that may arise from the mechanical damage and may result in an leakage of magnetic flux without applying external exciting field (hereafter, we call it a natural magnetic field)[3],[4]. This phenomenon shows a possibility to identify the mechanical damages by detecting the natural magnetic leakage flux. An obvious merit of such method is that the noise arisen from the surrounded structural component will not appear as there is no need to magnetize the material. A quantitative evaluation of damage is also possible if the correlation of the magnetizations and the local damage state is clarified and stored as known knowledge bases.

In view of the background stated above, the correlation of mechanical damages and the corresponding natural magnetization is investigated in this work by detecting the leakage flux density nearby the surface of a test-piece in which mechanical damages are introduced by using a tension or a fatigue testing. An advanced film type flux-gate (FG) sensor[5], which is efficient for a weak static field, is applied in the experimental system for measuring the natural magnetic field that is usually in a same order or even less than the magnetic field of the earth. The natural magnetic fields are measured both during the mechanical testing (in-situ) and after unloading (off-situ). In practical, the experiment is performed in a procedure as follows: at first, the phenomenon of the natural magnetization is demonstrated for SUS304 stainless steel by using standard test-piece and tensile testing. Then, the magnetic flux leakages were measured during and after the tensile testing for the same kind of test-piece under cyclic tensile loading in order to investigate the correlation of the natural magnetization and damages of plastic deformation. To evaluate the possibility of the damage status inspection for a key structure component in practical environment, signals of the magnetic leakage flux are measured during the fatigue testing. In this case, the distribution of the leakage magnetic field is measured at selected loading step numbers in an off-situ state for studying the evolution of damages at different fatigue stage.

On the other hand, though the flux leakage method is considered efficient for the ferromagnetic material, there is still no report for its application to the nonmagnetic/paramagnetic materials [3]. To clarify this question, the magnetic properties such as the residual magnetic field of a damaged material need to be known. As such measurement can be performed

with the same experimental setup by just adding a magnetizing procedure (for instance, using a permanent magnet), this is also chosen as a testing subject of present experiment.

This report consists of 4 sections. In the section 2, The details of the experiment (experimental set-up, principle, procedure, and etc.) are described. The experimental results are given in the section 3 for the tensile, fatigue and testing with magnetizing procedure respectively. The related discussions of the experimental results are made in the section 4. In the last part of the report, concluding remarks and some possible prospect work are given.

2. Experimental Issues

2.1 Test material and test-pieces

Aiming at application of the new flux leakage method to the NDE of structural components of new generation nuclear power plants, e.g. a plant of Fast Breeder nuclear Reactor (FBR) or that of the thermal fusion reactor (for instance, ITER), the stainless steel of SUS304 type is chosen as the target material to be inspected in this study. In order to perform zero-tension fatigue testing, a standard button type CCT test-piece[6] is selected considering the condition of our material testing system. 24 test pieces are fabricated from a raw material plate with the test-piece axis in parallel with the rolling direction. The present material is being used in the experimental FBR plant MONJU for taking advantage of its high performance in a high temperature environment. The chemical composition the material and the shape of the test piece is shown in Table 1 and Fig.1 respectively. The gauge region is the central part of the test piece that is in a plate geometry and sized 40 mm×20 mm×5 mm. For several test-pieces, through central notches (3 mm × 0.3 mm slit or hole with 0.3 mm diameter) are fabricated by using the EDM technique for guarding the position of crack initiation. The location of the central artificial crack is illustrated in the Fig.1 by taking a slit as example. Concerning the compress loading in the fatigue testing at both room temperature and 650°C, the thickness of the test-piece is selected as 5 mm, i.e. a relative short and thick geometry is chosen for preventing buckling.

Table 1 Composition of the SUS304 A3 material (wt%)

C	Si	Mn	P	S	Ni	Cr
0.05	0.55	0.82	0.021	0.003	8.78	18.38

To measure the distribution of the macro-strain that is necessary for investigating the damage-magnetization relation, 2 sets of grating lines in a pitch of 0.08 mm have been etched to a 30 mm × 20 mm region on one of the planar surface of the test-piece for producing fringe pattern that is necessary in the moire method for the strain calculation[7],[8]. The grating lines are etched only with a 3 μm depth, which allows the strain measurement being performed without affecting the distributions of the strain and the magnetization. A glass grating mask is also made with use of the same grating pattern used for the test-piece surface. A fringe pattern will appear once this standard grating mask be overlaid on the surface of a deformed test-piece.

2.2 Measuring Method and Experimental Set-ups

a). Measurement of the magnetic field

To measure the magnetic leakage flux density induced by the mechanical damages, a sensor valid for small and static field is necessary. The Hall effect sensor is not feasible in this case as it can not work even in the measurement of the magnetic field of the earth. A SQUID (superconductor quantum interference device) is a very sensitive equipment for the weak magnetic field. Unfortunately, the necessity for a magnetic field shielding and the low

space resolution protect this device from to be applied to the present subject. On the other hand, a conventional flux-gate sensor that has a sensitivity between the sensors mentioned above also has a drawback of low space resolution.

Recently, a new kind of FG sensor has been developed by the Shimatsu Corporation based on the photolithography technique. The film sensor is in a square shape with a side length about 1.0mm. The sensitivity of this sensor is about 0.0001Gs that can answer the needs of present application. The principle of the FG sensor can be described simply as follows:

As shown in Fig.2, the sensor consists of a core, an exciting coil, and 2 pick-up coils. The pick-up coils are connected in a differential way that makes the output signal becomes zero if no any external field presented. Once the sensor is set into a magnetic field, the balance of the two pickup coils will be disturbed, viz., one of it will change to $V + \Delta V$ and the other becomes $V - \Delta V$ where the ΔV is proportion to the magnetic field component shown in the Fig.2. Consequently, a signal of $2\delta V$ will be read that depends on the intensity of the external magnetic field linearly if the frequency is not too large.

From the principle described above, one may worry about the effect of the exciting field of the sensor on the magnetic field of the test-piece as a residual field possibly to be caused in a magnetic object when an exciting current moves over it. Fortunately, considering the fact that the excitation magnetic field is small and mainly concentrated in the ferrite core of the sensor, the effect from its leakage can be neglected for the problem we are dealing with. This fact is demonstrated when we perform a scanning near a surface of a demagnetized test-piece in which a slit exists. In fact, there is no significant perturbation detected near the slit. Therefore, omitting the effect of the exiting field is reasonable.

b). Measurement of the macro-strain distribution

As well known, the optical method is effective for the measurement of the strain distribution though it may give a lower precision than the method using a strain gauge. Considering the objective of the present experiment, say, investigating the homogeneity of the strain distribution during a simple tensile testing for the test-piece stated above, a method using moire fringe pattern is chosen.

The principle of the moire method is simple. At first, 2 sets of fine grating lines are printed on the surface of the test piece before deformation and the same grating lines are also printed on a standard glass mask. A fringe pattern will appear when the standard grating mask is overlaid on the deformed test-piece and the strain can be calculated by using the following formula,

$$\varepsilon_x = \frac{1}{f_x}\frac{\partial N_x}{\partial x}, \quad \varepsilon_y = \frac{1}{f_y}\frac{\partial N_y}{\partial y} \tag{1,2}$$

$$\gamma_{xy} = \frac{1}{f_x}\frac{\partial N_y}{\partial x} + \frac{1}{f_y}\frac{\partial N_x}{\partial y} \tag{3}$$

where, $f_x = M_x/L_x$(lines/m) with M_x the total number of the grating lines in the x direction, L_x the length of the grating region in the x direction and the same for the y subscript case. The sensitivity of this method depends on the pitch Δ of the printed grating lines as the minimum strain detectable is $1/M$. Though the numbers of the fringe lines

N_x, N_y are integer values, it can be treat as real variables by using a proper interpolation method.

For practical testing, the fringe patterns are caught after unloading the test piece unlike the situation shown in the schematic diagrams of Fig.3 concerning the difficulty of the in-situ measurement. The image of fringe patterns is converted into digital data through a CCD camera of 500,000 pixels and a high speed image board, and the strain distribution is calculated with a data processing code based on the formulae above on a personal computer. The setup of the moire method system is shown in the Fig.4 where the test-piece and glass mask (standard grating) is set on a specially designed instrument which can ensure the relative position and orientation of the glass mask and the test-piece which is important for enhancing the measuring accuracy.

c). In-situ measuring system of magnetic field

Fig.3 shows a flow-chart of the in-situ measuring system. 6 film type flux-gate sensors are set to the measuring point by using a specially designed instrument, which fixed at the topside of the test-piece as shown in Fig.5 to detect the magnetic field change during the tensile and fatigue testing (in-situ). A Shimatsu material testing machine (No AF-40) is applied as the mechanical loading system. The load limit of the machine is 5 ton and the maximum stroke is 50 mm. The sensors are fixed to the upper side of the test piece that does not move during both the tension and fatigue testing. The location of the sensors related to the test piece is shown in the Fig.6 and the lift-off of the sensors is taken as about 0.5 mm by adjusting the micrometer of the fixing instrument. The location of the sensors can also controlled by using another 2 micrometers, in other word, the fixing instrument allows the sensors to be arranged to any space point (of-cause the moving area of the sensors is limited considering the range of the micrometer). Though the fixing instrument allow the sensors to be set for measuring both the component in-plane and that perpendicular to the plate surface, we choose the in-plan component to measure as it can be performed with a smaller lift-off. The output of the sensors are transferred to the computer with use of a special amplifier and a data acquiring system called Thermo-Wave. The post processing of the measured data is performed on the personal computer using commercial codes and that specially developed during this study.

d). Off-situ 2-d scanning system

The distribution of the leakage magnetic field is measured off-situ by scanning the unloaded test-piece on a x-y stager. The experimental setup is shown in Fig.7. After magnetic field measurement, the plastic deformation is measured by catching the moire fringe patterns.

The scanning area is selected as a square region with side lengths of 30 mm. Being the same with the case of the in-situ measurement, the lift-off is chosen as 0.5 mm for the scanning of the horizontal components. In the case of the vertical component measurement, the practical lift-off is larger than the distance between the sensor and the test-piece surface considering the size of the sensor itself. The scanning path is like that shown in Fig.6 but with the pitch in the x direction chosen as 1 mm. As the stager is not an automatic one, the movement of the stager needs to be driven by hand with a screw system. The pitch along the axial direction of the sensor is not a constant that can be determined from the

speed of the scanning and the sampling system. The flux density at the data point with pitch of 1 mm both in the x and y directions are obtained by interpolating the measured data numerically.

e). System for magnetizing the test piece using a permanent magnet

To investigate the residual magnetization property of the test piece during a cyclic tensile testing, the test piece needs to be demagnetized/magnetized at each loading cycle. Magnetizing the test piece under the same conditions is necessary for realizing the research objective. Considering this requirement, the following magnetizing procedure is chosen that enable the the difference of the residual field due to the magnetizing system to be minimized.

At first, the test piece is set to the instrument that is designed for the position control in the strain measurement (the moire method). The instrument then was put on the table of the x-y stager with the center of the test piece coincided with that of the permanent magnet but with a different z coordinate. This operation is used to ensure the setting instrument to be set at the same location for each magnetizing step, which can be realized by adjusting the permanent magnet first to the center of the test-piece and then moving off perpendicularly to a position far away. Before each loading step, the test piece is demagnetized and arranged to the same position of the instrument referring the counter of the equipped micrometers. Setting the instrument to x-y table at the position determined in the first step (according to the marks made on the table of the x-y stager), the relative position of the magnet and the test-piece can be ensured with a high accuracy. For magnetizing the test-piece, the permanent magnet is moved downward at first to a position touching with the test-piece surface, and then set to a $50\mu m$ lift-off. The permanent magnet is moved then in a path of $(x, y) = (0\text{ mm}, 0\text{ mm}) \rightarrow (0\text{ mm}, -20\text{ mm}) \rightarrow (0\text{ mm}, 20\text{ mm}) \rightarrow (0\text{ mm}, 0\text{ mm})$, and finally moved up vertically to a far position. Though the magnetization is not uniform for this magnetizing method, the residual field does not change a lot for different magnetizing step if virgin test-pieces are used.

In this work, a permanent magnet consisting of 3 cylinder magnets (length: 3 mm, diameter: 5 mm, $B_r \simeq 0.1$T) is employed. The axis of the magnet is set in parallel with the axis of the test-piece. The setup of the magnetizing system is shown in Fig.8.

2.3 Experimental Procedure

The number of the utilized test-pieces and their testing conditions are summarized in table 2. The test-pieces are demagnetized by using an electromagnetic demagnetizer (Hozan HC-21) before setting them to the material test machine. Strain control is applied for all the tensile and fatigue testings. In case of the tensile testing, the flux density at the central part of gauge region is in-situ detected while the distributions of the leakage magnetic field are measured on the x-y stager after unloading the test-piece. For the test-pieces of number NDT14 and NDT12, they were unloaded after each ε_{max} (see Table 2) was reached for magnetic field distribution measurement with the 2-d scanning. In case of the fatigue testing, the in-situ measuring of the magnetic field is performed with the sensors set at the same locations used in the tensile testing for all the loading cycles. However, the 2-d scanning for the distributions of magnetic field is performed only for the test-piece

that was unloaded at given cyclic number. Once a crack initiated, the fatigue testing can be stopped automatically according to a threshold minimum loading value set beforehand.

The measurement of the 2-d distribution of the strains is only performed for the test-piece NDT14 and NDT13. The unloaded test-piece is set to the specially designed instrument, and the glass mask is overlaid. The moire fringe patterns were taken into the computer and the fringe line information was extracted by processing the obtained image data i.e. calculating the discrete values of the $N_x(x,y), N_y(x,y)$. The strain is calculated then by using a code based on the Eq.(1) and Eq.(2). This procedure is carried out for each loading step listed in the table 2 for NDT14. The results show that the strain measured by the push type strain sensor agrees well with that obtained by the moire method, which in turn shows that the local concentration of deformation is not significant for these two test-pieces and loading patterns.

Table 2 Measured test-pieces and their test conditions

No. of Test-Piece	Central Notch	Experimental Conditions
ndt2	no slit	ε_{max} = 3%, 6%, 9%, Loading speed 0.01%/sec
ndt21	slit	ε_{max} = 3%, Speed: 0.01%/sec
ndt14	no slit	0.2%, 0.5%, 1%, 2%, 3%, Speed: 0.01%/s
ndt12	no slit	0.2%, 0.5%, 1%, 2%, 3%, 6.0%, Speed: 0.01%/s
ndt21	slit	Range: ± 0.25%, Speed: 0.1%/sec, N=1, ∼ 940
ndt20	slit	Range: ± 0.25%, Speed: 0.1%/sec, N=1, ∼ 980
ndt14	no slit	Range: ± 0.25%, Speed: 0.1%/sec, N=1, ∼ 4600
ndt13	slit	Range: ± 0.25%, Speed: 0.1%/sec, N=1, ∼ 63000

3. Experimental Results

3.1 Results of the tensile testing

a). Measuring results of the flux density

Fig.9 shows an in-situ measuring result for test-piece NDT2 during a tensile testing from 0% to a maximum strain of 3%. The test conditions are listed in the table 2 where 3%, 6%, and 9% mean that the test-piece was unloaded after total strain 3%, 6%, 9% was reached respectively. The results shown in the figure is the case during the tension to 3%. From this result, it is clear that the magnetizations have occurred in the gauge region. As the test-piece was demagnetized before the tension and there is no external magnetic field changed during the testing, such a magnetization is obviously caused by the applied deformation or loading. On the other hand, though small magnetic fields have been detected at the elastic period, the magnetization increases much faster when plastic strains occurred, and saturate at last when the plastic deformation getting too large. In addition, the magnetization did not disappear after the loading was released. These results tell us that the magnetizations arise from the plastic damages but not from the effect of inverse magnetostriction. Fig.10 shows the in-situ measuring results for the NDT2 test-piece during tension from 2.8% (the residual strain of the first tensile testing) to 5.8%. It is clear that the change of the detected flux density is much smaller than that happened for the virgin material test-piece, or in other word, a saturation has happened in this case.

To investigate the property of the magnetization distribution, the 2-d distributions of the leakage flux density have been measured after unloading the test-piece. Fig.11 gives the distribution of the B_y component of the flux leakage at a plane 0.5 mm over the test-piece surface (lift-off 0.5 mm). A large magnetic leakage can be found at the bottom side of the test piece that shows a valley pattern inclined with the axis of the test-piece. This phenomenon associates us with a possibility of a global plastic slipping i.e. Ludas band. In other word, as we consider the magnetization arises from the damages of plastic deformation, more plastic damages may exist in the bottom side of the test-piece. To investigate the damage state of this test-piece, small samples are cut out from the unloaded test-piece after the 3rd tensile cycle (from ε_r=5.55% to ε_{max}=8.55%). As a result, it was found that the number of slipped grains at the bottom side is about 2 times over comparing with that at the topside. The detail observing results of the microstructure will be given in the following subsection.

Fig.12 depicts the B_y distribution of the test-piece NDT2 unloaded after maximum strain 5.8% was reached. One can find that there is no much difference from that shown in the Fig.11. This result agrees with the conclusion obtained from the in-situ measurement, i.e. the magnetization did not change much for the plastic deformation of a high level as a result of the saturation.

If the peaks of the flux density detected at the bottom side of the test-piece is a result of the slipping lines, the distribution of the magnetization at the tips of the slit after a tensile testing is of interesting for the verification of this conjecture. For this purpose, a tensile testing was applied to the test-piece NDT21 with the maximum strain selected as 3%. Fig.13 shows a in-situ measuring result of the B_y. Comparing with Fig.9, it is obviously that the detected flux density is much smaller than that of the case of NDT2.

In addition, the distribution of B_y did not show significant difference in the vicinity of the crack tips. This result can be explained as that, though there is local slipping near the tips of slit, the magnetization did not change a lot because the slipped grains did not gather in same direction like the case of the test-piece NDT2 (the difference of the local and global slipping). This difference may comes from the the loading history, the geometry of the test-piece or the random property of the material grains. From this point of view, the assumption that a global slipping can led to a large magnetization does not conflict with this experimental result.

b). The microstructure of the test-piece NDT2 after large tensile deformation

As mentioned in the previous subsection, small samples are cut out from the test-piece NDT2 from selected positions as shown in Fig.14. For all the samples, observations using a normal optical microscope are performed at first. In the Fig.15, the microstructures at positions along the central line of the test-piece (top side, bottom side and in the button region) and at the edge of the test-piece (top side and bottom side) are given. No much difference was identified in the volume fraction of the δ ferrite phase at the top side, bottom side and at the button region (virgin materials). However, content of the ferrite phase is different at different rolling lines (the volume fraction at the central site is larger than that at the edge part) for the test-piece NDT2. Therefore, though the δ phase exists for a virgin SUS304 material, its volume fraction is not so large (less than 1%) and may not be uniform.

Table 3 Comparison of the number of the slipped grains

Region	Position	Number of locally slipped grains
Bottom side (peak region)	edge site	32
	central site	71
Top side (weak region)	edge site	16
	central site	36

To investigate the difference of the microstructure between the top side and the bottom side of the test-piece NDT2, a scanning electronic microscope (SEM) is also utilized in the observations of the samples mentioned above. Fig.16 shows images of SEM for 2 samples taken from the top and the bottom of the gauge region respectively. It is clear that local slipping have taken place at many grains. The slipping lines are in two patterns crossed each other with a slipping angle of about $\pm 25°$. For considering the effect of the local slipping, the numbers of the slipped grains at the samples of the top side and the bottom side were counted under an optical microscope. Table 3 gives some results about the number of the slipping grains. The number at the bottom side is about 2 times over comparing with that at the top side.

Considering the nonmagnetic property of the austenitic phase in the SUS304 material, slipping lines shall not result in a natural magnetization directly excepting those occurred in the grains of δ phase. However, as the magnetic field is much larger at the bottom side where slipping lines have a higher density, some magnetic phase may nucleated in the austenitic area, say, a martensite transformation may occurred[9]. To conform this conjecture, a higher resolution observation is also performed by using a transmission electronic microscope (TEM). Fig.17 shows an example of the TEM images at the bottom side of the

the gauge region. From Fig.17(a), one can find some special zones (black region) appeared at the positions where 2 sets of slipping lines cross each other, Fig.17(b) is a zoom in image of this special zone. Fig.18 gives the x-ray diffraction images at these positions. It is clear that the special zones in the Fig.17 are martensite phase as they have a bcc crystal structure. This means that the martensite transformation is a practical phenomenon for SUS304 material even under a simple tensile loading and at a room temperature.

c). The results of the moire method

From the results described above, it is possibly that the natural magnetization is mainly caused by concentrated plastic deformation such as the effect of the ludars band. However, it is not easy to understand the local concentration of deformation for the present testing conditions as it is approximately a plan stress problem if the affect of the grain size and the thickness of the test-piece can be omitted

To investigate the correlation between the magnetizations and the macro-strain, the distribution of the strain is measured by using the moire method as described previously. A typical fringe pattern for the test-piece NDT14 unloaded after the tension to maximum strain of 4.4% is shown in the Fig.19. From this figure, it is difficult to find that a concentrated deformation has occurred during the tensile testing. Actually, the results from the moire method agree well with that measured from the push type strain sensors as shown in table 4. Other measurement results of the NDT14 after cyclic tensile loading and those of NDT13 after fatigue testing support this assumption. On the basis of these results, one can not deny the possibility that a global slipping may led to a large natural magnetization. Actually, the flux density for the test-piece NDT14 and NDT13, in which no local deformation is found, is also very small. However, even for this case, the occurrence of the magnetization has also been verified.

Table 4 Comparison of the strains measured by the moire method and the strain sensor

Moire method	0.35%	0.91%	2.05%	3.52%
Strain sensor	0.36%	0.95%	2.19%	3.78%

Fig.20 and Fig.21 depict the in-situ measuring results of test-piece NDT14 during tension with strain range 0.08% $\sim$ 0.5% and 0.35% $\sim$ 1.08% respectively. The magnetization has been induced again though it is much smaller than that of the test-piece NDT2. However, the magnetization is in the same order with that measured from the test-piece with a central slit (NDT21). In other word, the magnetization in a small magnitude can be induced even in case that there is no global slipping band occurred. In this case, this magnetization can be considered as a result of the anisotropy in the δ phase grains of the SUS304 material that may be caused by the dislocations and other mechanical damages from the plastic deformation.

3.2 Results of the Fatigue Testing

a).The results of the test-piece with central slit

To investigate the affect of a fatigue crack on the natural magnetization, zero tension fatigue testings have been performed for the test-piece NDT21 (with a residual strain of

about 2.8%) and NDT20 (virgin material). The testing conditions listed in the Table 2 were applied at a room temperature. For the test-piece NDT21, through fatigue cracks of about 3mm were initiated after about 900 cycles at both the two tips of the central slit. The distribution of the flux density B_y measured after unloading is shown in Fig.22. From the figure, it is easy to find that a significant magnetic field signal was detected at the vicinity of the fatigue crack. On the other hand, fatigue cracks of about the same length also have been initiated at the tips of slit after about the same cycles for the test-piece of virgin material. The distribution of the flux density for this case is given in Fig.23, from which one can find that the magnetizations are induced again nearby the fatigue cracks. Comparing with the results shown in the Fig.22, the magnetization for a virgin material test-piece is smaller than that of the test-piece with a residual strain. Based on these results, one can conclude that a fatigue crack in a SUS304 structure component can be recognized nondestructively by monitoring the leakage signal of the natural magnetic flux.

b). Magnetizations near the fatigue crack

Visualizing the distribution of the magnetization at vicinity of the crack is important for investigating the principle of the magnetizing procedure and is also necessary for validating the code for inverse analysis, which is necessary in the prediction of the magnetization distribution in the material from the measured flux density signals. As a jointed study of a research committee of the JSAEM named "the research committee for the electromagnetic fracture and its application to the nondestructive evaluation", the feature of the material nearby the fatigue crack was investigated by observing the surface magnetization with a magnetic colloidal method and by observing the surface distribution of the magnetic grains using the magnetic force microscope (MFM) for samples cut from the central part of the test-piece NDT21. The work was performed by the group of prof. Nakasone of TUS (Tokyo University of Science) with cooperation with groups at the national institute of metals of STA and the Mechanical Engineering Laboratory of the MITI Japan. Fig.24 shows a result of the colloidal method where the distribution of the magnetization in the vicinity of the fatigue cracks is illustrated [10]. From the figure, it is clear that the magnetizations mainly localized nearby the edge of the fatigue crack. In other regions including the region near the central slit, the magnetization is not significant. This result agrees with the prediction of the inverse analysis summarized in the first réport of this work [11] and the inversion results of the measured data using a neuronetwork approach [12].

To investigate the distribution of the magnetic phase in the material near the crack, the MFM [10],[13] was used to visualize the microstructure at the test-piece surface and in the material. The measurements were performed after the interested region being cut out and polished by mechanical means. In order to reduce the affect of the mechanical machining, a further chemical polishing is also carried out. Fig.25 shows the position of the selected areas of the MFM scanning and Fig.26 gives a typical MFM image near the crack edge in case without chemical polishing. It is easy to find that, unlike the image obtained in the region far from the crack region, a maze like magnetic domain structure is clearly observable. This result tells us that even for the paramagnetic material like SUS304 steel, a magnetic domain structure is also possibly exist when fatigue damages was introduced, or in other words, magnetic phase is possibly transformed to a high volume fraction in the vicinity of crack. However, as the maze like magnetic domain is usually considered as a

result of the mechanical polish, a chemical polishing is also applied for observing the real structure of magnetic domain induced by the mechanical damages. Fig.27 depicts a result of MFM observation for the same area shown in the Fig.24 for the test-piece after chemical polish. A cross slipping line system can be recognized in this figure, and a relative high force region can be found at the cross point of these slipping lines. This result agrees well with the observation result of the test-piece with tensile deformation, i.e., the martensite transformation is caused by the mechanical damage (slipping) at the region of the crack occurred during the crack propagation. As there is no similar magnetic domain structure was verified at a position far from the fatigue crack, one can consider the plastic deformation induced martensite transformation may only happens for a plastic strain of a high level.

c). Fatigue testing results for test-pieces without slit

For clarifying the evolution of the magnetization before the crack initiated, test-pieces without central slit are also applied to the fatigue testing. Unlike the experiment of the test-piece NDT21 and NDT20, the in-situ signals during the fatigue testing are also measured. The introducing of a high accuracy A/D converter makes this possible as the data acquiring system used for the NDT21 and NDT20 is a relative old version one which has a precision even smaller than the magnitude of the natural magnetic field signals.

For test-piece NDT14, which has been applied in the cyclic tensile testing as described in subsection 3.1(c), the fatigue testing was terminated automatically at a cyclic number of about 4600 as the test-piece broken at a unexpected position (the top of the planar region where a small initial defect happened due to a failure in the fabrication of the grating lines). Therefore, the behaviors of the magnetization during crack initiation has not been caught. Fortunately, this defect is not fatal for the result of the tensile testing described in the last subsection as the defect is not significant and is far from the gauge area. Fig.28 shows a typical wave form of the detected flux density signals at the starting period of the testing with a comparison to that of the test-piece NDT13. The magnetic field changes with the oscillated deformation in the period of the applied loading (strain) though a phase different between them and a double period component can be recognized.

In case of test-piece NDT13, the fatigue experiment was performed successful until a fatigue crack initiated in the gauge region though it is not at the central area. The testing was suspended at cyclic numbers of 2000, 4000, 7000, 10000, 13000, 16000, 19000, 37200, and 54300, and the distributions of the flux density B_y were measured at these cyclic numbers for the unloaded test-piece that was performed carefully in order to terminate the testing at a state of zero strain (the strain monitored by the push type strain sensor). There is no significant magnetization change was conformed in the distribution of magnetic field in these 2-d scanning. This means the damage induced magnetization is smaller the the environment noise at least. Consequently, detecting the damages state before crack initiation is difficult by scanning natural magnetic field without using a shielding or other means for enhancing S/N ratio. After restarting the fatigue testing from cyclic number 54300, the test machine was stopped at cyclic number 63007 automatically as threshold value of the minimum loading was reached. After unloading, a tiny surface crack of about 2mm long was observed at the upside of the test-piece. In this case, a little perturbation can be distinguished in the distribution of the magnetic field though it is much smaller than that of the case of NDT21 and NDT20 (Fig.29).

Fig.30 shows the time history of some typical signals detected from the test piece NDT13. At the beginning of the testing, a relative large magnetic field change was found in its direct component. However, this change was saturated at about 10 cycles though a change at the amplitude of the magnetization wave can be identified. To show the phase change of the magnetic field signals and that of the strains, the hysteresis curves of the measured magnetic field signal are plotted versus the applied strain and stress referring the method used for fatigue detection based on the magnetostrition penomenon[14]. As examples, Fig.31 shows the hysteresis curves at the cyclic number of 10, 620, 3700, 7000, 19000 and 63000 versus the applied strain and Fig.32 shows those versus the applied loading (stress). From Fig.31, it is easy to find that the area of the hysteresis curves increased with the increasing cyclic number. In the curves just given, the affects of the noise was reduced with a simple filtering operation, i.e., the high frequency noise is reduced by taking the signal as the summation of the neighboring sampling points (5 points were used) and the low frequency noise was reduced by just summing up the signals with those at the neighboring periods.

Comparing the signals of the virgin test-piece with that obtained from the test-piece with residual strain, one can find that the main different is the wave form (Fig.28). The peak value due to the tensile load is obviously smaller in the case of the virgin material.

3.3 Results in case with a magnetizing procedure

The results described in the previous sections are data for natural magnetic field. It is found that the field value is not large if considering its application to the damage inspection. In other word, though the method using natural magnetic field can be used to identify the fatigue cracks and even possibly to be used for its classification and sizing, the inspection of the damages is no easy as the signal is in a same order with the magnetic field of the earth and even smaller. This means that the noise at a practical environment may makes the signals of 2-d scanning being polluted and may led to a unbelievable inspection result.

Instead of applying the natural magnetic field to evaluate the damage status, another possibility is to measure the magnetic coefficients of the deformed material like what has been done for the magnetic materials [3], i.e. to detect the damage in the nonmagnetic/paramagnetic material with a similar way with that used for the ferromagnetic materials. For this purpose, the magnetic property of the test-piece NDT12 with different plastic damages was investigated by using the same loading procedure with the test-piece NDT14 and the magnetizing method described in the previous section. In practical, the test-piece was demagnetized at first, and a permanent magnet was used to magnetize the test-piece then with the procedure described in subsection 2.3(e). The leakage magnetic flux of the magnetized test-piece was measured before setting it to the loading system. Having applied strains to a maximum value listed in the table 2, the test-piece was unloaded and the distribution of the magnetic field was measured again. This procedure then was repeated for each tensile cycle of the NDT12. From this experiment, the behaviors of the magnetized test-piece under tensile and fatigue loading, and the evolution of the residual magnetic field for different plastic damages can be obtained.

Fig.33, Fig.34 and Fig.35 show the distribution of the magnetic field after magnetizing the demagnetized test-piece NDT12 that has been loaded to a maximum strain of 1.0%,

2.0% and 6.0% respectively. The figures for the other strain cycle are not given here as the results for the maximum strains less than 2.0% is almost the same with that for the virgin material. In addition, it is also verified that the residual magnetic field for different test-piece does not change much. However, after 2.% strain applied, the B_r begin to get larger. As shown in the Fig.33, the maximum $B_{r,y}$ becomes over-range though the magnetizing procedure is just the same. On the other hand, the $B_{r,y}$ did not change much after 200 fatigue cycles of a 0.5% strain range were applied to the test-piece NDT12 (after tension to strain 6%).

Figs.36 $\sim$ 39 show the in-situ measuring results of the changes of the flux density for the magnetized test-piece. One can find from these results that a significant change of magnetization occurs due to the plastic deformation. Unlike the effect of the inverse magnetostriction [14], the signals of the detected magnetic field shows an irreversible property. In the Fig.34 and Fig.35, the magnetic field changed in the elastic region is very small comparing with that occurred at the area of the plastic deformation. However, for the elastic deformation of the test-piece with residual strain, the magnetization in the material changes with the applied loadings. In other word, the magnetization does not variate proportion to the plastic deformation but depending on the strain in a similar pattern of the stress-strain relation. However, the magnetization is irreversible if one notice that the magnetization did not decrease much when the loading released. It is also can be find that the proportional limit of the stress corresponds to the proportion point of the signal of the flux density signal in case of a large residual strain (more than 1.0%).

Fig.40 gives the in-situ signal of the magnetic field during fatigue testing for the test-piece after tension to 6.0% and magnetized with the permanent magnet. The direct component of the magnetic field changes rapidly at the first several loading cycles and then becomes slower. The amplitude of the vibrated signals is also getting smaller with the increasing cyclic number. Comparing with the magnetic field of the tensile testing, one can find that they change with a similar pattern. This means that the properties obtained from the tensile testing may applied to the test-piece subject to fatigue loadings.

4. Discussions

4.1 The principle of the natural magnetization

Based on the experimental results described in section 3, the principle of the damage induced natural magnetization can be considered as the follows:

For the simple tensile testing of a relative lower strain range, the magnetization occurs mainly due to the anisotropy caused by the plastic deformation, or in other words, due to the plastic damages in the test-piece such as the dislocations and slipping lines in the grains or at the grain edges [15],[16]. The damages affect the direction of the axis of easy magnetization and make the spontaneous magnetization in the grains of magnetic phase changing direction to the easy axis with a higher possibility. Actually, as shown in the previous sections, grains of the δ ferrite phase exist in the SUS304 stainless steel though its volume fraction is not so large comparing with the austenitic phase. These magnetic grains is considered as the source of the paramagnetic property of this material. A magnetic domain structure may occurs in these magnetic grains and its direction may be affected by the anisotropy of the material. Once dislocations or slipping occurred due to a plastic deformation, some domain walls will be moved in order to make the total potential being minimized that may led to the natural magnetization. However, for the tension of a large strain, the martensite transformation is also possibly happen that can led to an extra natural magnetization considering the volume fraction increment of the magnetic phase.

This explanation of the natural magnetization is reasonable considering the phenomena we find in the experiments. The occurrence of the large magnetization of the test-piece NDT2 can be considered as the result of a large local slipping and the martensite transformation. A global slipping (Ludas band, not only slipping in grains) may result in a strong anisotropy in the test-piece. However, the occurrence of global slipping is not only depending on the conditions of the plastic deformation. A local microstructure and the loading history may also affect the formation of the global slipping band. This is the reason why there is no large natural magnetizations observed for the other test pieces, say, there are no global slip lines happened for test-piece NDT21, NDT14 and NDT2. If there is no global slipping lines occurred, the natural magnetization will be small as the slipping lines in the grains may take different directions as shown in the observation results of the microstructure (Fig.16). On the other hand, the results of the flux density in the magnetized test piece is much larger than that for the demagnetized ones. This can also been explained by the conjecture above. In this case, the magnetic domain walls are moved due to the energy of the external magnetic field, which enables a global magnetization. Once damages are introduced by a mechanical energy, some domain walls will move back or to the easy axis as the present direction is not stable that makes the detected leakage flux density decreased. Considering the coexistence of the two sets of slipping lines that is crossed each other, this decrement is not difficult to be understood.

In case of the fatigue cracks at the tips of the central slit, the principle of the natural magnetization is a little different. In this case, in addition to the magnetizations induced with the same mechanism of the tensile testing, the martensite transformation occurred near the fatigue crack as a result of the cross slipping and mechanical energy may plays a

major role of the natural magnetic field. Of cause the increment of the magnetic phase is not equal to more natural magnetic field because of the random orientation of the spontaneous magnetization of the magnetic domains. However, as the anisotropy is more significant than the simple tensile testing considering the stress concentration, more magnetic phase can led to a large natural magnetization. This can be considered as a reason of that the natural magnetic field at the crack vicinity of the deformed test-piece is larger than those of the virgin material.

Actually, from the observation results of the magnetic colloidal method and the MFM, the possibility of the martensite transformation in a fatigue testing is conformed. Though the results of the colloidal method only can show that a large magnetization exists in the vicinity near the crack, whether it is from the slipping or the martensite transformation can not be distinguished. However, from the results of the MFM image, one can say that the magnetic phase exists in a much larger volume fraction comparing with the area without stress concentration and the area of virgin material. This can be considered as an evidence of the martensite transformation. In fact, the TEM observation of NDT2 supports this consideration. Actually. the martensite transformation of the NDT2 can be considered being caused by a tension-tension fatigue testing of 3 fatigue cycles.

4.2 The correlation of the magnetization and the plastic strain

Excepting the test-pieces with a global slipping and those magnetized using a permanent magnet, the magnetization signals are very small and even weaker than the magnetic field of the earth. The change of the magnetization is mainly occurred at the first stage of the plastic deformation, i.e. the natural magnetization will saturate when the plastic deformation gets too large. Fig.41 shows the flux density change at tensile loading cycle (different residual strain) for test-piece NDT14 and NDT2. It is obviously that the change of the magnetization in a test piece with high residual strain is much smaller than that happened in the virgin material.

As the natural magnetization is possibly affected by the state of the local deformation, (for instance, the magnetization of a test-piece with global slipping is much larger than that in a test-piece with same or more residual strain), it is not easy to apply the signal of the natural flux density to quantitative prediction of the state of the macrostrain, or the state of the mechanical damage of the plastic deformation. However, considering the fact that the magnetization do changes with the increasing mechanical damages for all the situations, the detection of the flux density signal is a possible way for monitoring the change of the state of the mechanical damages since a global slipping is hard to take place in the practical structural component. However, even for such applications, efforts for reducing the environment noise is also important.

4.3 Correlation of the fatigue damages and the feature parameters of the detected magnetic field signals

From the measured 2-d distribution of the leakage magnetic field for the test piece unloaded during the fatigue testing, it is difficult to identify fatigue damages from the detected signal as the signal of the magnetization is very small and is polluted by the

environment noise. This means that a 2-d scanning of the natural magnetic field may not gives a valuable information related to the status of the fatigue damages. However, if we compare the time history of the magnetic flux density, one can find a significant difference for signals of test pieces in different residual strain. This tells us that some feature parameters of the detected signals may connect with the damages, which consequently, can be used as the parameter to monitor the damage state of the test piece[14].

Fig.42 gives an evolution of the area of the hysteresis curve of flux density versus the applied strains (see Figs.31,32) and Fig.43 shows the change about the signal of the sensor 1. From these results, it is clear that the area increases rapidly at the first stage of the fatigue life. After about 10,000 cycle, the increment of the area becomes slower. On the other hand, Fig.44 gives a corresponding evolution procedure of the amplitude of the flux density signals. Unlike the area of the hysteresis, the amplitude does not change much at the first stage but increase linearly at the last period of the fatigue life. From these result, we can say that the area of the hysteresis curve is a suitable parameter for monitoring the fatigue damage, i.e., if the change of the area getting slower, which means the fatigue life limit is approaching.

4.4 The possibility to detect plastic damages from magnetic material parameters of the SUS304 steel

Fig.45 shows a correlation of the maximum residual flux density for the test pieces with different residual strain. From the figure, we can find that the maximum residual magnetization did not change a lot for the residual strain of 1% or smaller. For the residual strain greater than 2%, the $B_{r,max}$ gets large linearly. This phenomenon can be considered as the effect of the the martensite transformation as it can make the volume fraction of the magnetic phase gets larger, which in turn, can led to the increment of the residual magnetic field of the damaged material. From this point of view, the residual magnetic fields is possibly to be applied to the prediction of the volume fraction of the martensite phase, or in other words. the plastic damages can be identified nondestructively by monitoring the residual magnetic field if the damage state is not too small.

Considering the similarity of the mechanical damages from the tensile plastic deformation and from the fatigue testing, one may guess that the fatigue damage can also be detected by measuring the residual magnetic field. In other word, the maximum residual magnetic field is possibly to be used to predict N/N_f for a fatigue loading in small strain range, though it may not be sensitive at the first stage of the fatigue life.

In table 5, the proportional limit of the of the $\varepsilon \sim \sigma$ and $\varepsilon \sim B_y$ curves are summarized. The maximum changes of the magnetic field of the 6 sensors for the loading cycles described in the section 3.3 are also listed in the table. The definitions of the $\varepsilon_p, \varepsilon_{py}$ and B_y^{max} are depicted in Fig.46. From this table, one can find that these 2 proportional limits are nearly the same for test-piece with residual strain over 1%. In addition, the change of the magnetic field during the tensile testing also stop to increase after 1% tensile strain was applied. These results show that the mode of damage may change at a plastic strain within tensile strain 1% $\sim$ 2%. Actually, this phenomenon agrees with the change of residual magnetic field and the saturation phenomenon of the natural magnetization.

Table 5 Comparison of the proportional limit ε_y of the $\varepsilon \sim \sigma$ curve and ε_{by} of $\varepsilon \sim B_y$ curve, and B_y^{max}, the change of the magnetic field during tensile testing to ε_{max}

	0.2%	0.5%	1.0%	2.0%	3.0%
ε_y (%)	0.107	0.122	0.157	0.165	0.188
ε_{by} (%)	0.2	0.213	0.153	0.151	0.182
B_y^{max}(Gs)	0.23	0.50	0.62	0.62	0.64

4.5 The possibility to detect damage by using the natural magnetization

From the experimental results and discussions given in the previous subsections, we can find that though the natural magnetic field is useful in the detection of a large fatigue crack, it is not easy to be applied to the evaluation of the damage state by scanning the natural magnetic field during a in-service inspection. However, it is possibly to be applied for monitoring the change of the damage status by set a magnetic sensor to positions that are considered as the weak point of the key structure component. As the signal of the natural magnetic field is not so large, more efforts for enhancing the sensing system is necessary such as employing a shielding device for protecting the environment noise. On the other hand, the feature parameter (area of the $B \sim \varepsilon$ hysteresis curve for instance) proposed in the previous subsection is sensitive to the fatigue damage, and is possibly to be applied to a structure component subjecting to a transverse loading. However, this method also has a drawback, as the area of the hysteresis curve or the amplitude of the signals need the information of the loading or strain. Unfortunately, this information may be not available for problems such as a low cycle fatigue or damage of creep testing.

Unlike the method using the natural magnetic field, the method predicting the residual magnetic field is more robust against the environment noise as a result of the external magnetizing. In addition, the measurement of the residual magnetic field is easy to be performed as an in-service inspection method. A high space resolution of the measurement can also be realized by using a small exciting coil (or permanent magnet) coupled with a magnetic field sensor. However, the correlation of the residual magnetic field and the fatigue damage (N/N_f) needs to be demonstrated later for the SUS304 material.

5. Conclusions and Prospect Work

Based on the experimental results described in the previous sections and the discussions, the following concluding remarks are obtained,

1. Natural magnetizations occurs for the SUS304 stainless steel due to a mechanical damage especially at the vicinity of the fatigue cracks. The natural magnetic field can be considered as the results of a mechanical damage (from the plastic deformation or a fatigue testing). Therefore, the measurement of the natural magnetic field can be considered as an efficient method for the NDE of fatigue cracks as the noise from the magnetizing procedure can be removed. On the other hand, because of the saturation phenomenon and the affect of global slipping, detecting the status of mechanical damages before a crack initiated is difficult by scanning the natural magnetic field. However, the natural magnetic field can be applied in the monitoring of the damage status of a given point if the environment noise can be reduced by using a special measuring system.

2. The area of the field-strain hysteresis curve increases with the increasing fatigue cyclic number. The amplitude of the magnetic field signal is also getting larger especially at the last period of the fatigue life. These parameters can be applied to the online monitoring of the status of the fatigue damage for key structure components subjecting cyclic loadings.

3. At a room temperature, the martensite transformation is also possibly to be occurred for a relative large tensile loading. At the tips of the fatigue crack, a martensite transformation also possibly happens due to a cyclic loading even of a small strain range. The reason of the natural magnetic field can be considered as result of both the anisotropy due the plastic damage and the increment of the magnetic phase due to the martensite transformation.

4. The residual magnetic field changes significantly for a test-piece with large plastic deformation. However, at a low plastic deformation level, the residual magnetic field will not change a lot. This phenomenon may be applicable for the detection of the martensite transformation and the damage recognition for materials with large mechanical damage.

As prospect work, the following subjects are important:

1. Investigating the correlation of the N/N_f and the feature parameter of the measured natural magnetic field for various test conditions and test-pieces.

2. Checking the correlation of the maximum residual magnetic field B_r with the density of the martensite phase and the N/N_f parameter and evaluating the possibility to be applied to the detection of fatigue damages.

6. Acknowledgments

The authors would like to thank Professor Kenzo Miya of the University of Tokyo for his continuous encouragement and helpful discussions. The FG sensors used in the testing are provided by the Shimatsu Corporation. The helps from Mr. Fujiyama of Shimatsu Corporation are sincerely acknowledged. The authors owe special thanks to the members of the Research Committee of Electromagnetic Fracture Mechanics and Nondestructive Evaluation of JSAEM, especially professor Y.Nakasone of Tokyo University of science, for valuable discussions and providing the observing results of MFM and magnetic colloidal method. A sincere gratitude directs to Mr.Ishigami and Mr.Tomida of the JOYO Industry Ltd. for their helpful cooperation during the fatigue testings and the microstructure observations.

References

[1] R.B.Mignogna, and et al., Passive nondestructive evaluation of Ferromagnetic materials during deformation using SQUID gradiometers, IEEE Trans. Appl. Supercond., Vol.3, No.1, pp1922-1925, 1993.

[2] Report of research committee on electromagnetofracture and its applications on nondestructive evaluation of degradation and damages, JSAEM report, JSAEM-R-9803, 1998.

[3] A.Gilanyi, K.Morishita, T.Sukegawa, M.Uesaka, and K.Miya, Magnetic nondestructive evaluation of fatigue damage of ferromagnetic steels for nuclear fusion energy system, fusion engineering and design, Vol.42, pp485-491, 1998.

[4] K.Yamada, and et al, Nondestructive cross evaluations of iron-based materials by magnetic sensors and laser speckle interferometry, Proc. Int. Symp. Mag. Mater., 1998.

[5] Y.Yamada, and et al., Application of thin-file flux-gate sensor, New Ceramics, No.2, pp15-18, 1998.

[6] T.Kunio and et al., Experimental method for fracture mechanics, Asakura Publisher, 1984.

[7] B.Han, Recent advancements of moire and microscopic moire interferometry for thermal deformation analysis of microelectronics devices, Experimental Mechanics, Vol.38, No.4, pp278-288, 1998.

[8] Y.Morimoto and et al., Moire analysis of strain by Fourier transformation, Trans. JSME, Vol.54-A, No.504, pp1546-1551, 1987.

[9] Y.Ozaki and et al., Elementary Metallography, Asakura Publisher, 1978.

[10] Y.Nakasone, Collaborative study on a new magnetic nondestructive evaluation of degradation in a stainless steel, Proceedings of the MAGDA'Brisbane, 2000.

[11] Z.Chen, K.Aoto, and S.Kato, Passive electromagnetic NDE for mechanical damage inspection by detecting leakage magnetic flux, I. Reconstruction of magnetic leakage magnetic flux, JNC report, JNC TN9400, 99-061, 1999.

[12] S.Takaya, G.Perad, T.Demachi and K.Miya, Inverse analysis of magnetization distribution for diagnosis of non-ferromagnetic steel, Proceedings of the MAGDA'Brisbane, 2000.

[13] T.Suzuki and K.Hirano, Fatigue damage analysis of austenitic stainless steel by magnetic force microscope, Proceedings of ECF12, Vol.1, pp97-102, 1997.

[14] A.Yoshinaga, and B.Yoshii, Detection of torsion fatigue in steels by using the effect of magnetostriction, Trans. JSME, pp343-369,1977.

[15] S.Chikazumi, and et al., Hand book of magnetic material, Asakura Publisher, 1975.

[16] S.Takahashi, Correlation of magnetization and dislocation in the region approaching to saturation, Report JSAEM, JSAEM-R-9704, pp27-38, 1998.

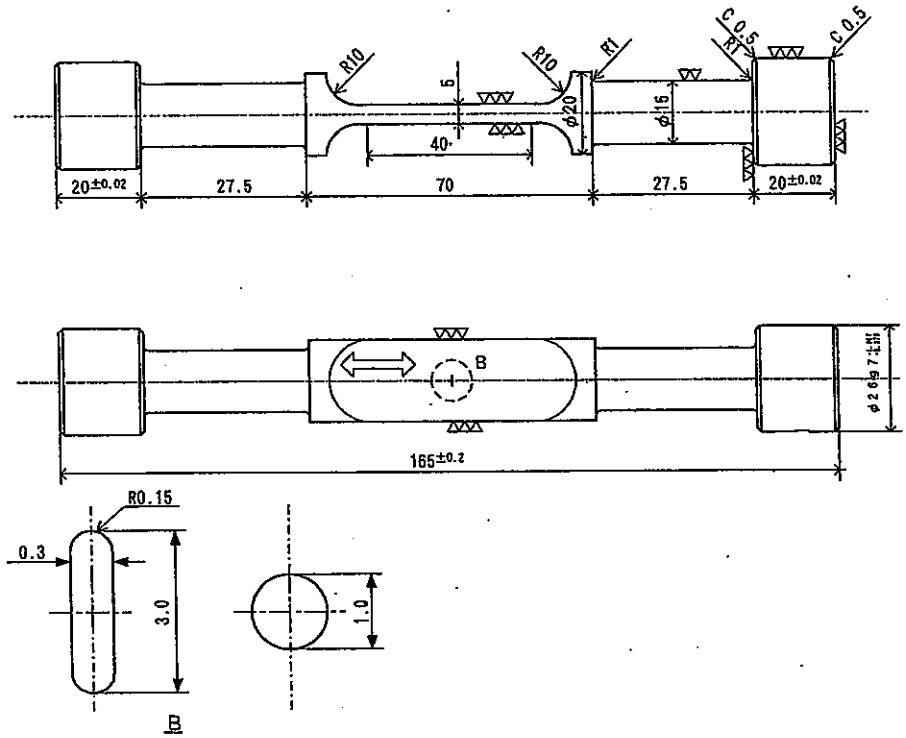

Fig.1 Shape of the botton type CCT testpiece

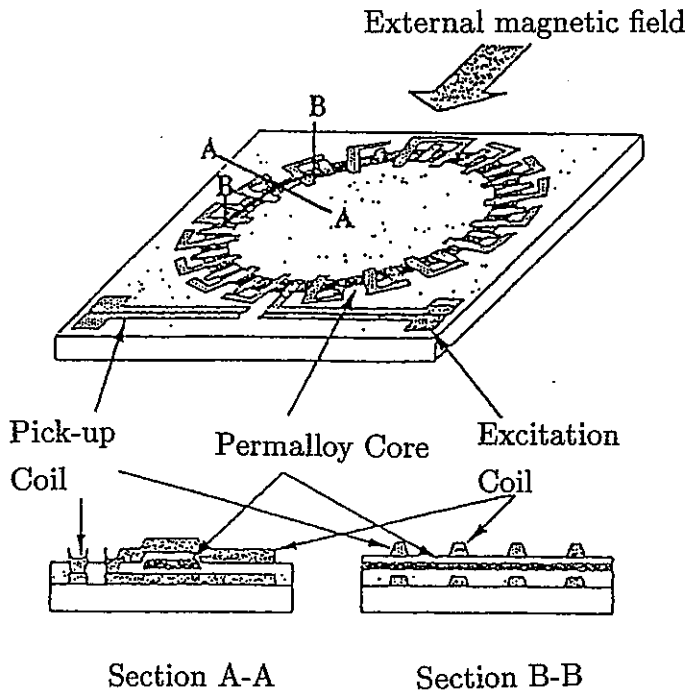

Fig.2 Principle diagram of the FG sensor

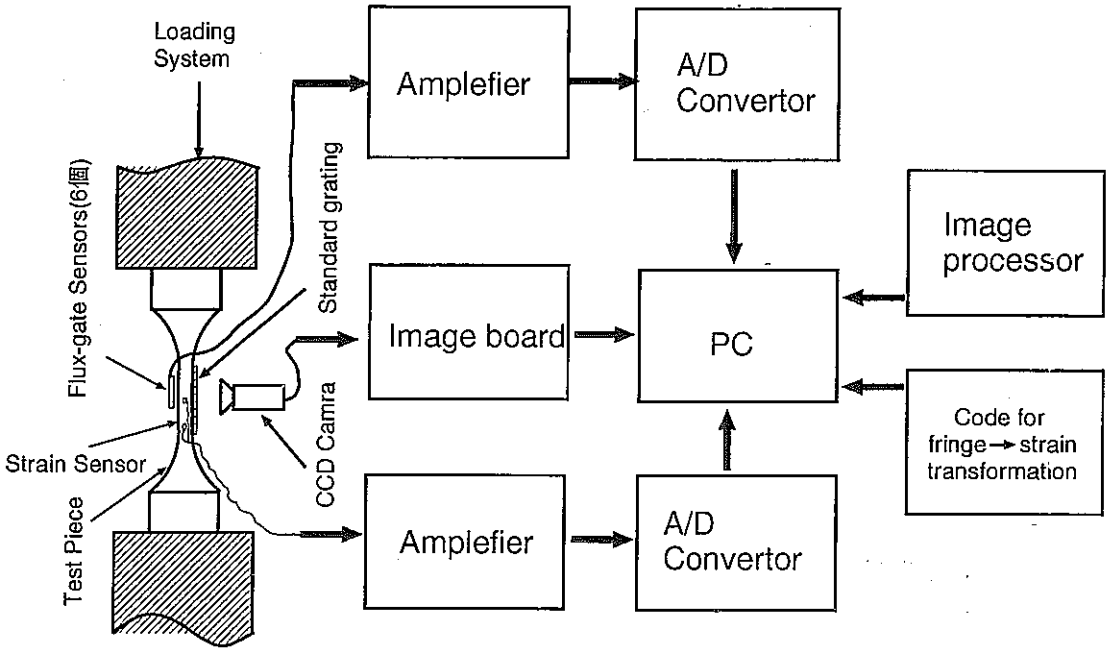

Fig.3 Schematic diagrams of the insitu measuring system

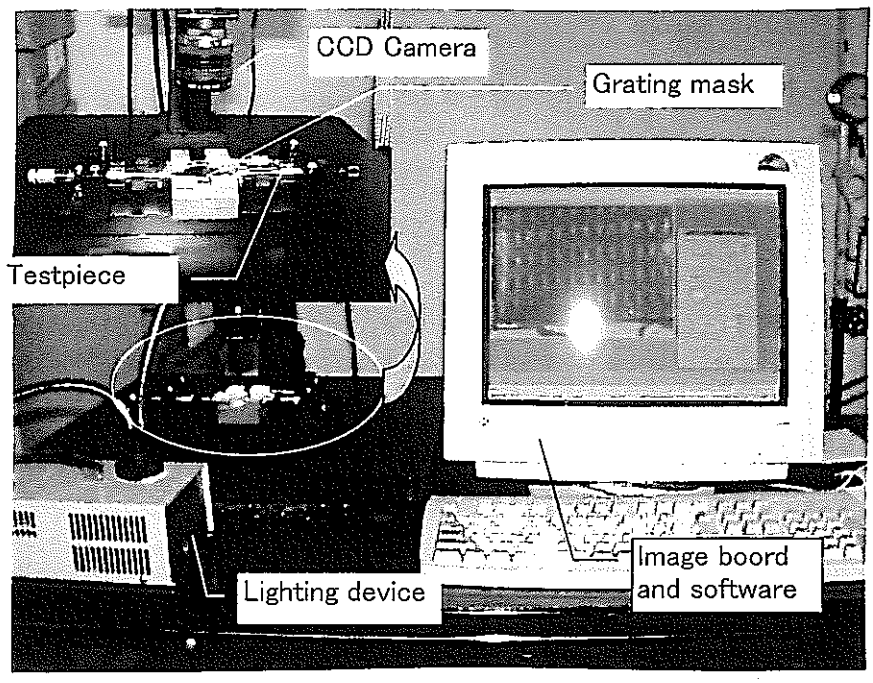

Fig.4 The measuring system of moire method

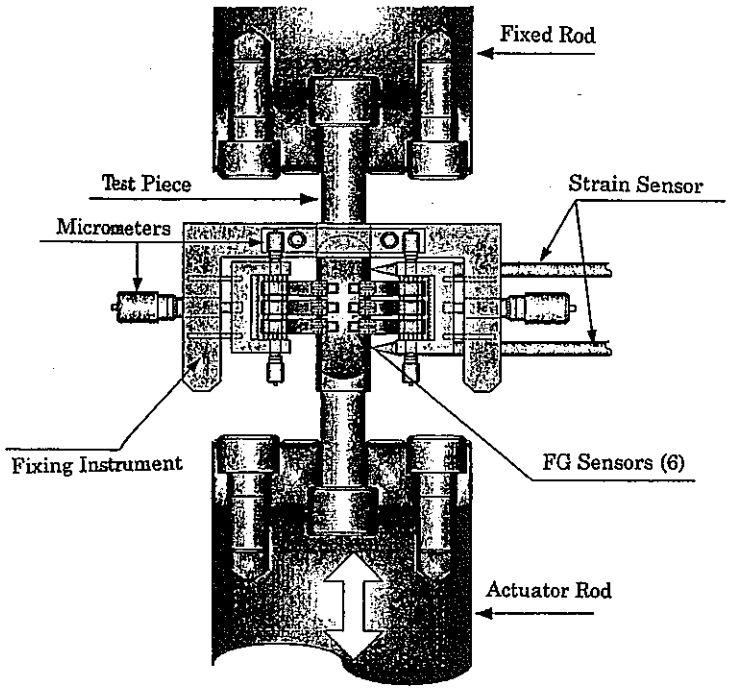

Fig.5 Fixing instrument for setting sensors

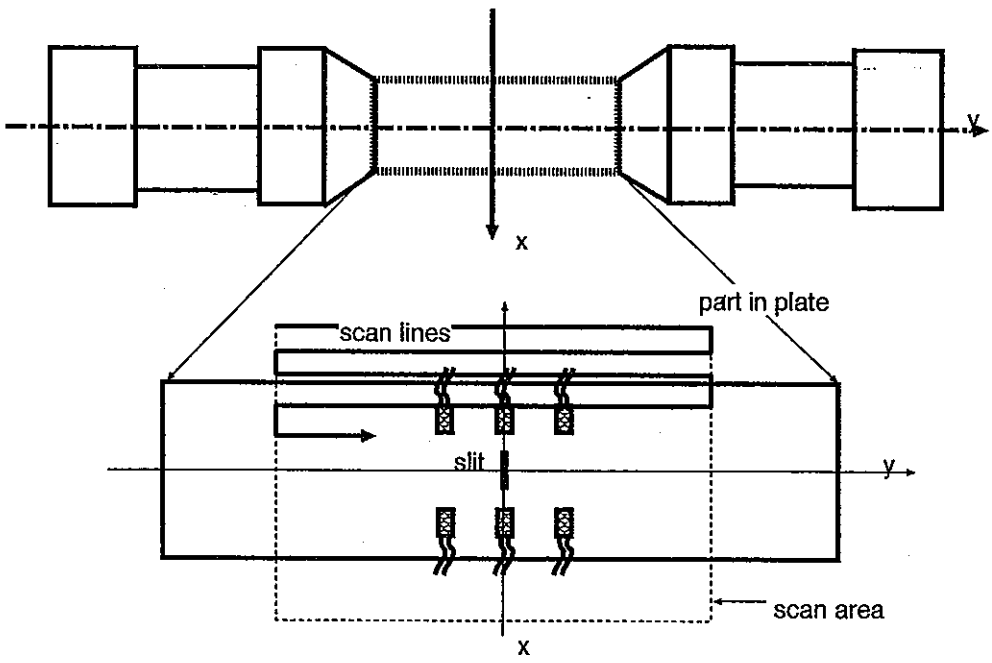

Fig.6 Setting locations of the FG sensors

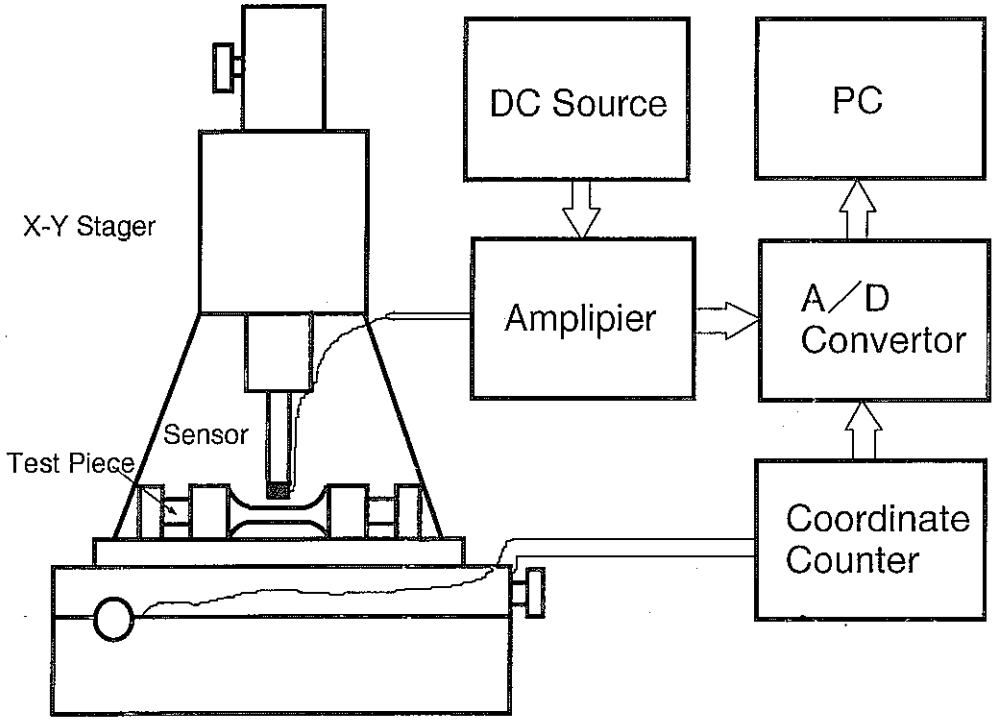

Fig.7 Experimental setup of the off-situ scanning system

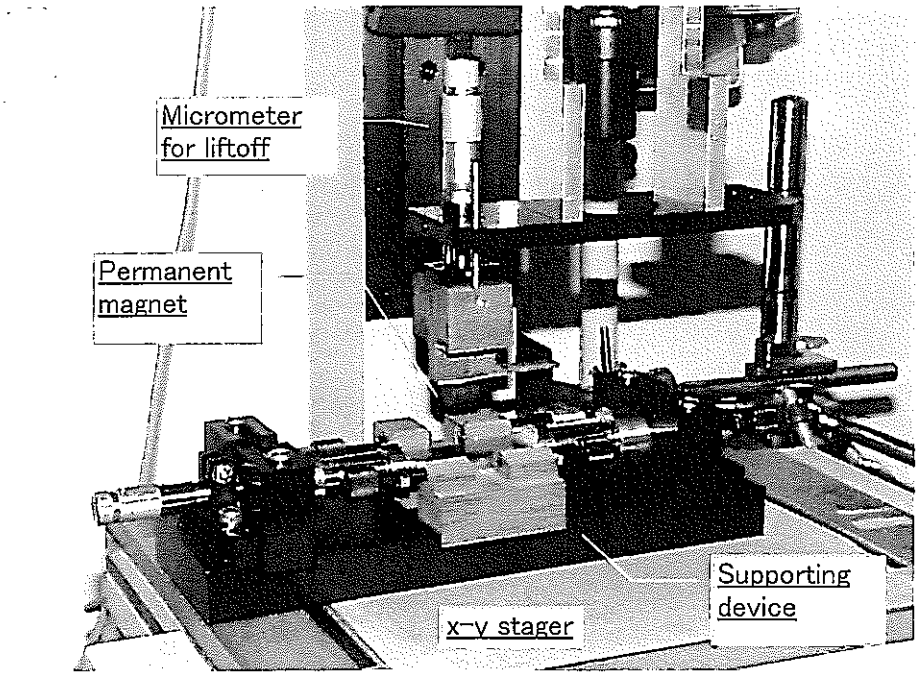

Fig.8 Setup of the magnetizing system

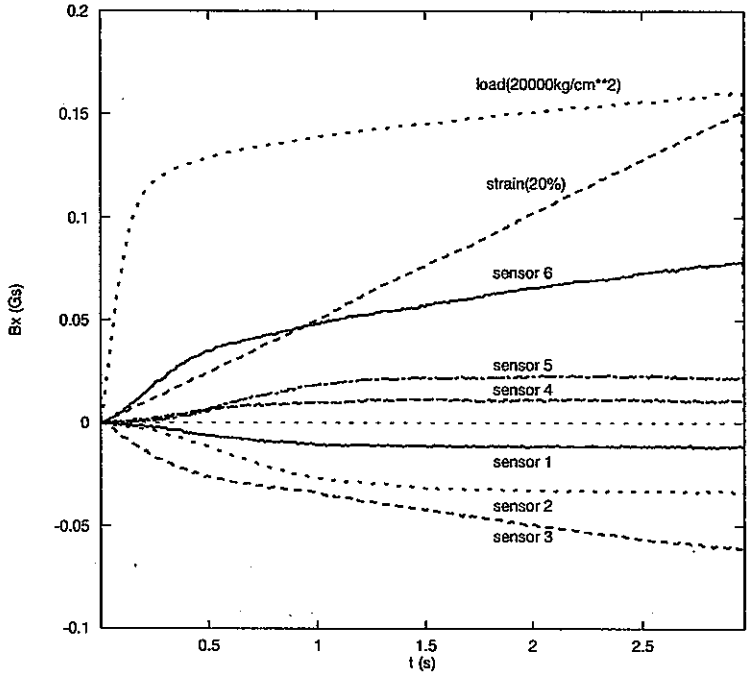

Fig.9 Insitu measuring result of NDT2 during tensile testing (0% ~ 3%)

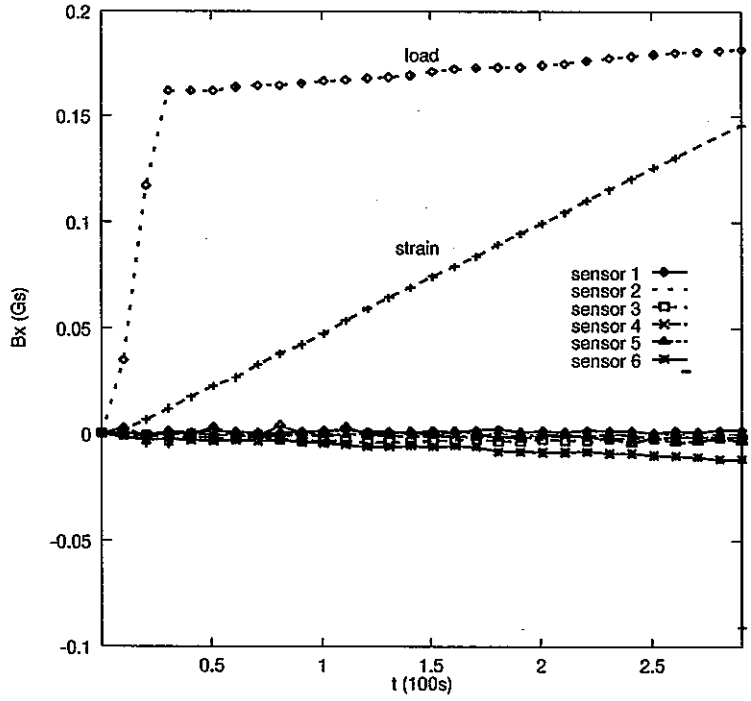

Fig.10 Insitu measuring result of NDT2 during tensile testing (3% ~ 6%)

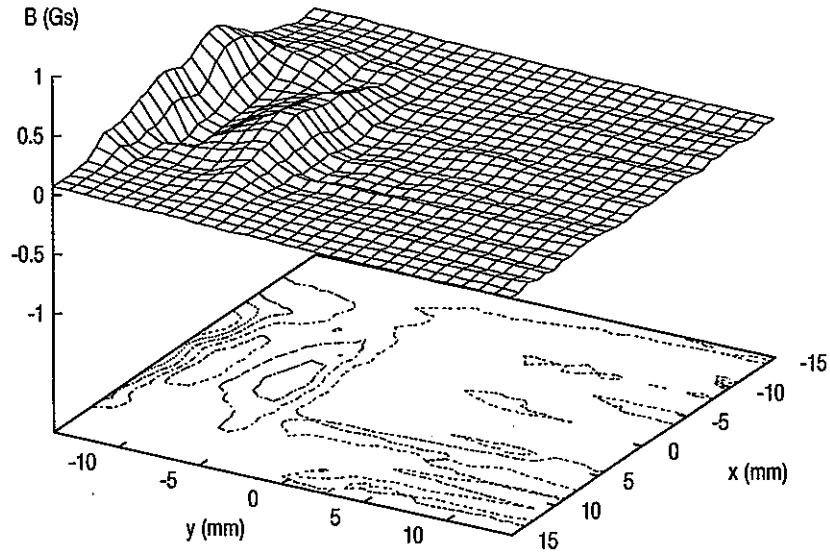

Fig.11 Distribution of the natural magnetic field after tensile testing
(NDT2, 0% ~ 3%)

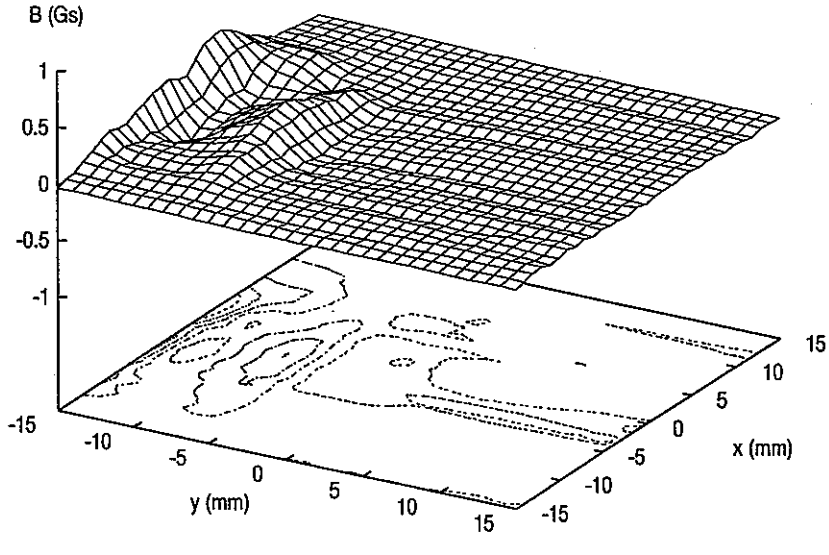

Fig.12 Distribution of the natural magnetic field after tensile testing
(NDT2, 3% ~ 6%)

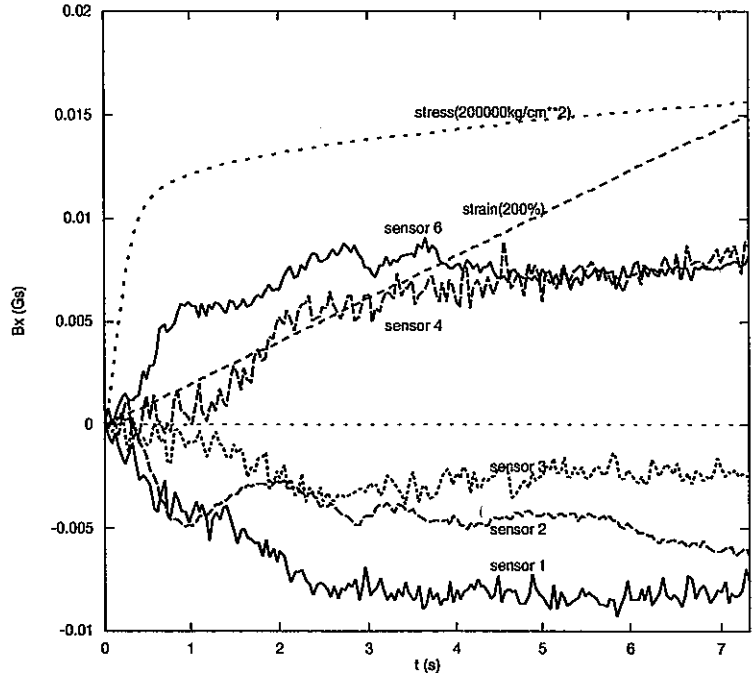

Fig.13 Insitu measuring result during tensile testing (NDT21, 0% ~ 3%)

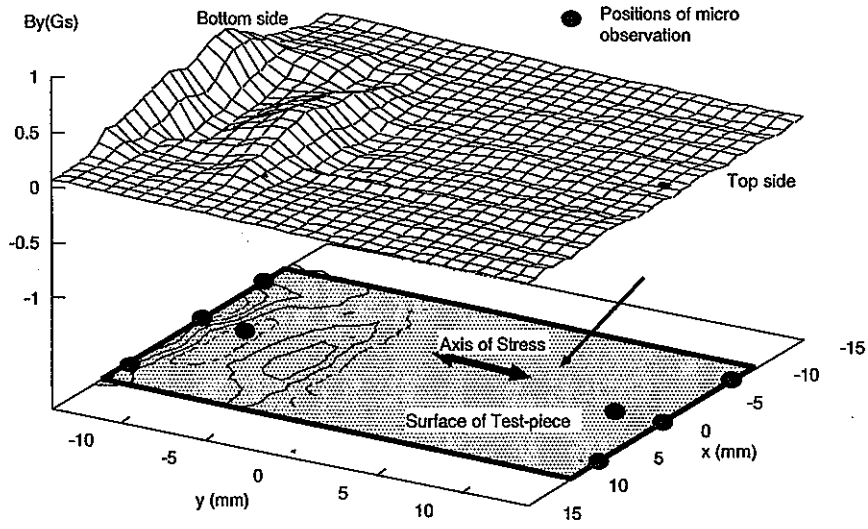

Fig.14 Location of the samples cut out from the testpiece NDT2 after tensile testing (NDT2, 6% ~ 9%)

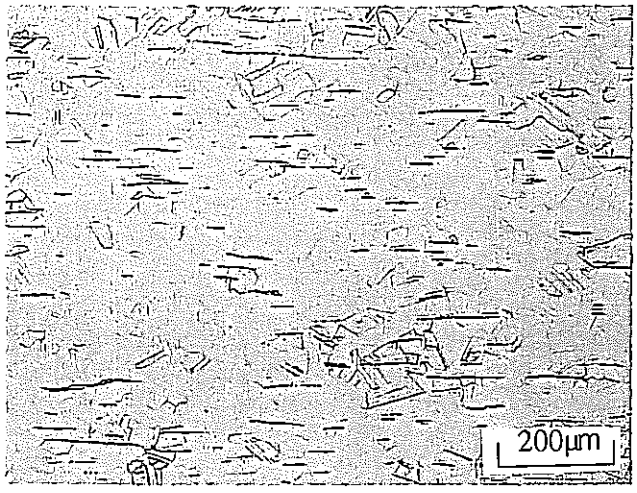

a). Center of the top side

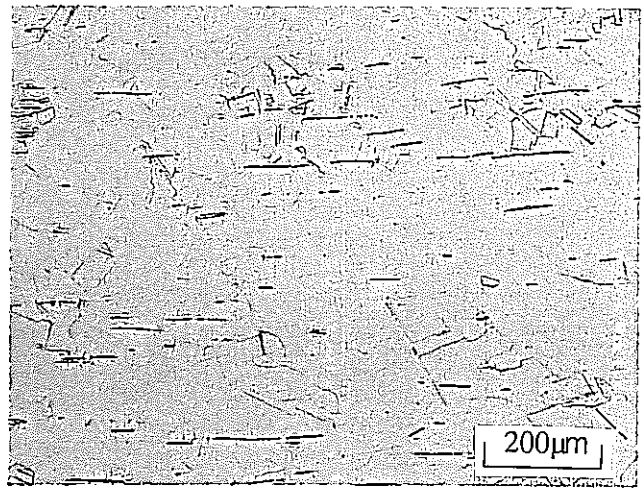

b). Right hand of the top side

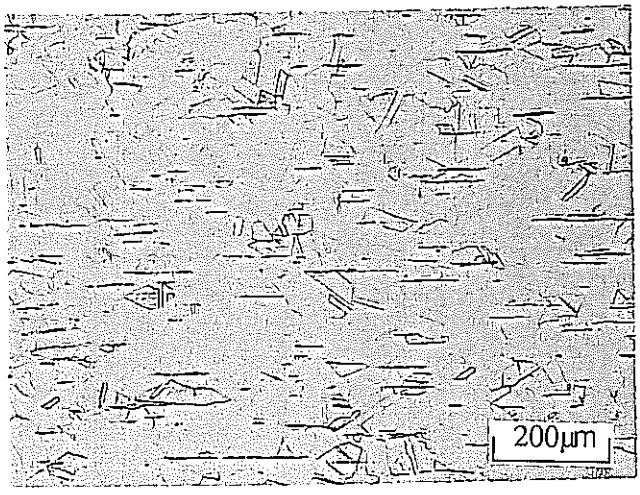

c). Center of the bottom side

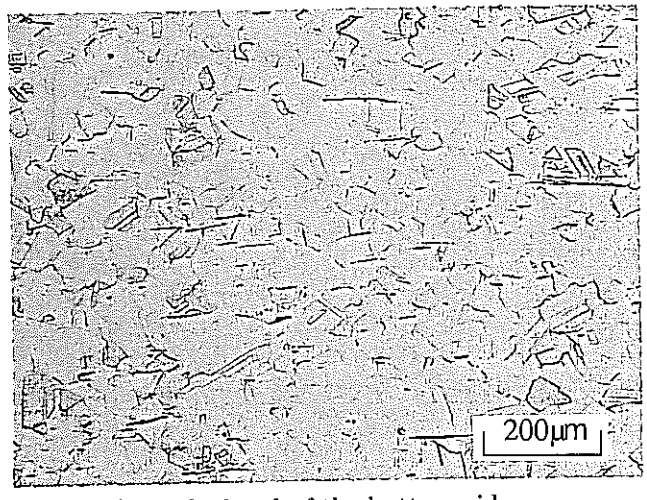

d). Right hand of the bottom side

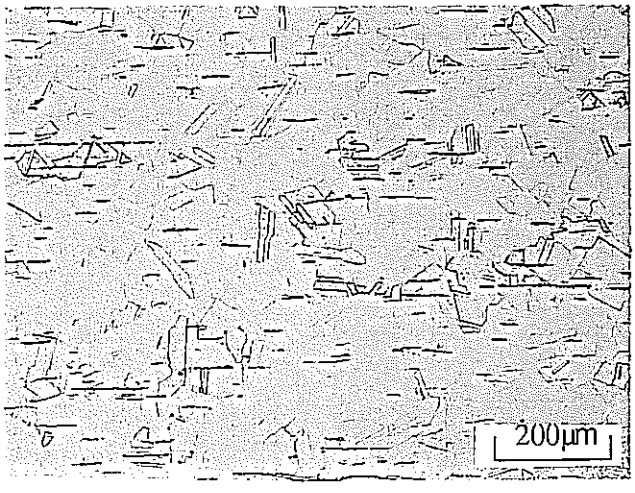

e). Vrigin material

Fig.15 Comparison of the microstructure of the samples taking out from different positions (NDT2, after 9% tension)

Sample at the top side

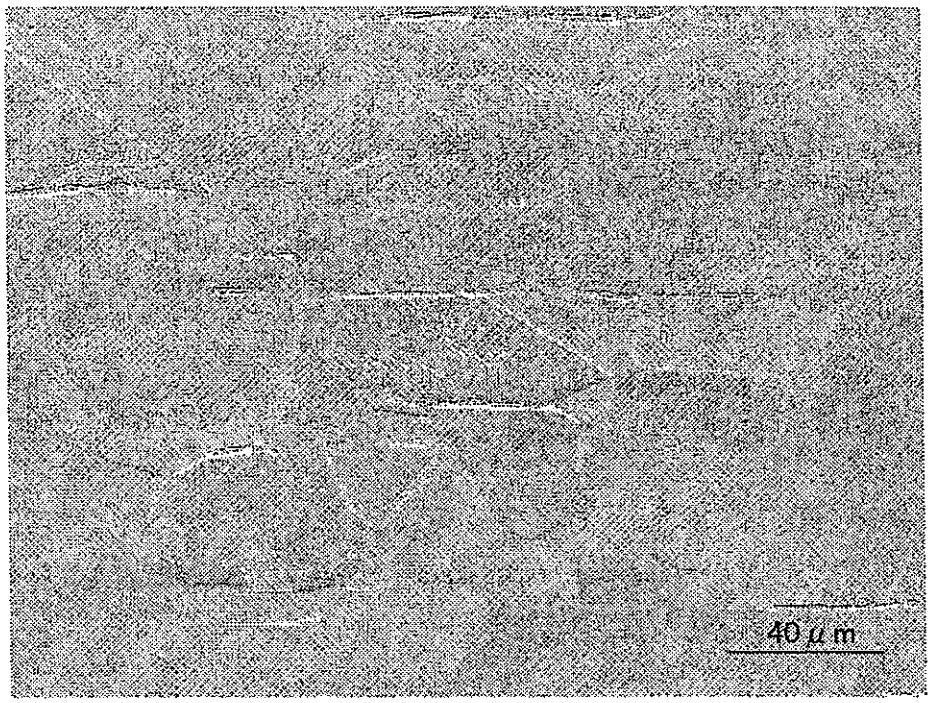

Sample at the bottom side

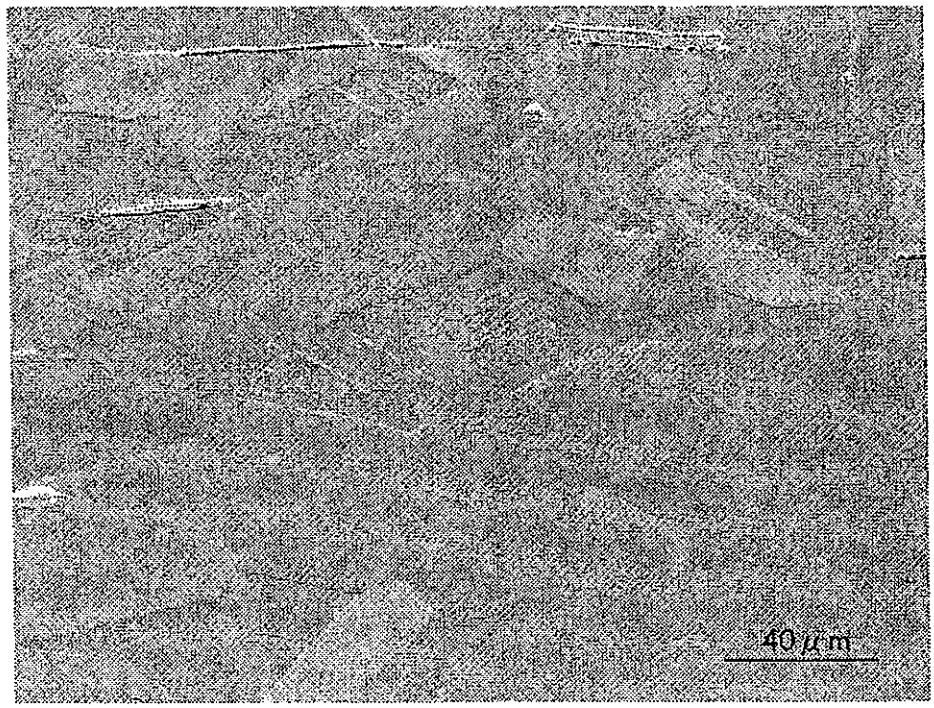

Fig.16 Comparison of the local slipping of the sample at the top and bottom side of the tesepiece NDT2 (after 9% tension)

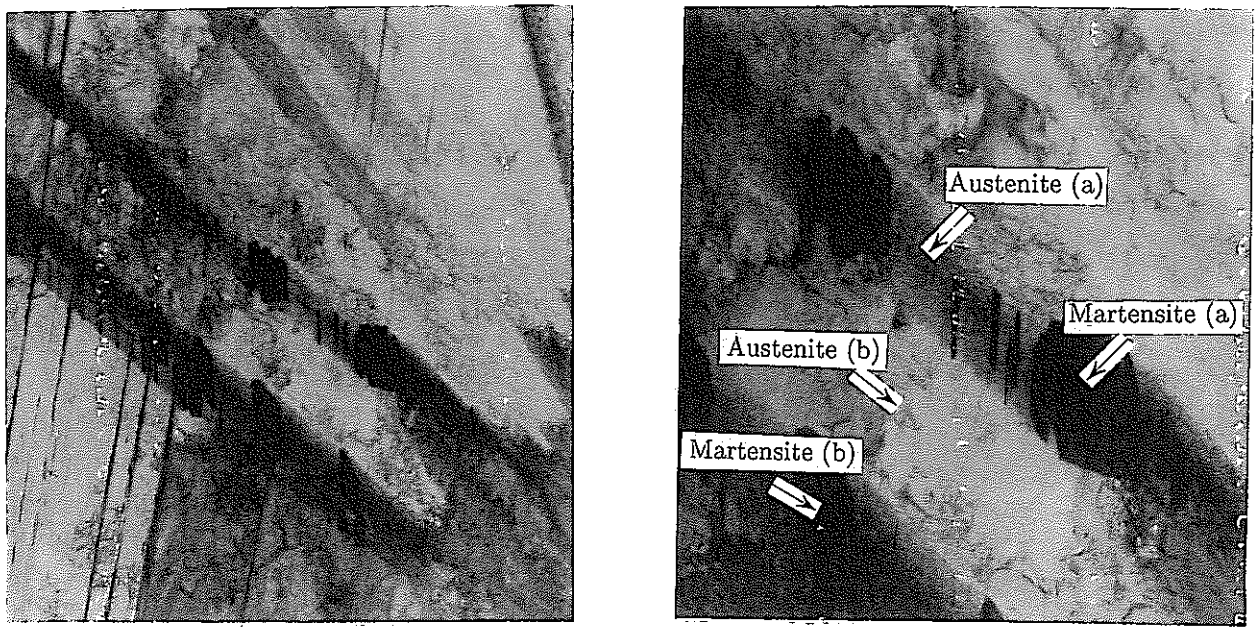

Fig.17 TEM image of sample cut from the bottom side of the tesepiece NDT2 (after 9% tension)

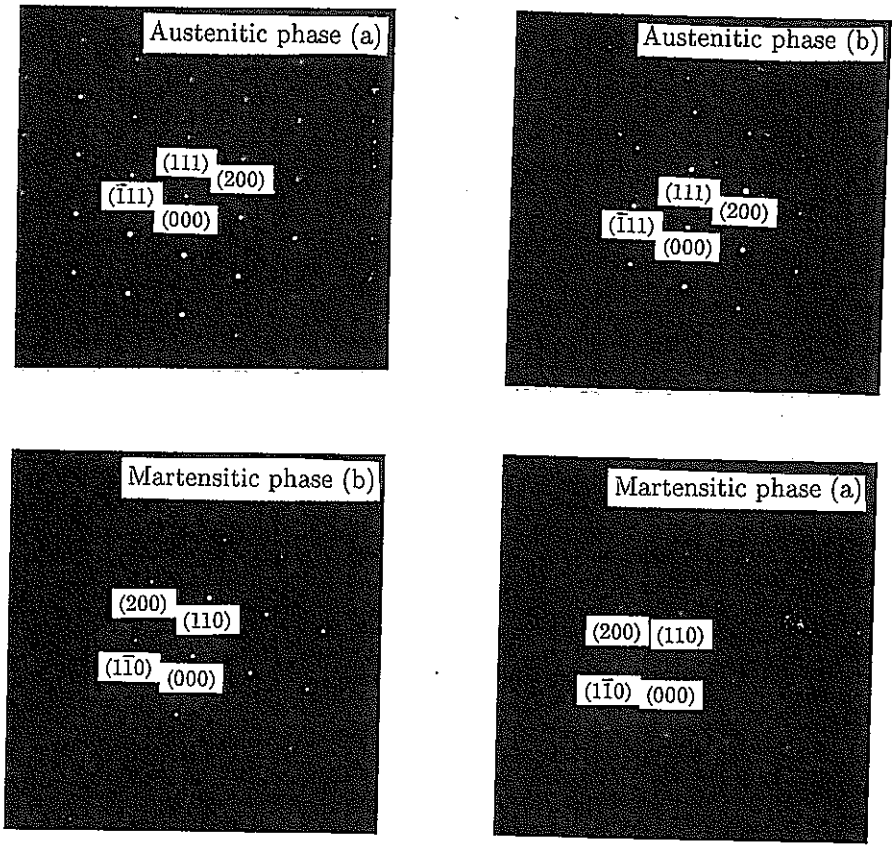

Fig.18 X-ray diffraction images for determining the property of the various phases shown in the Fig.17

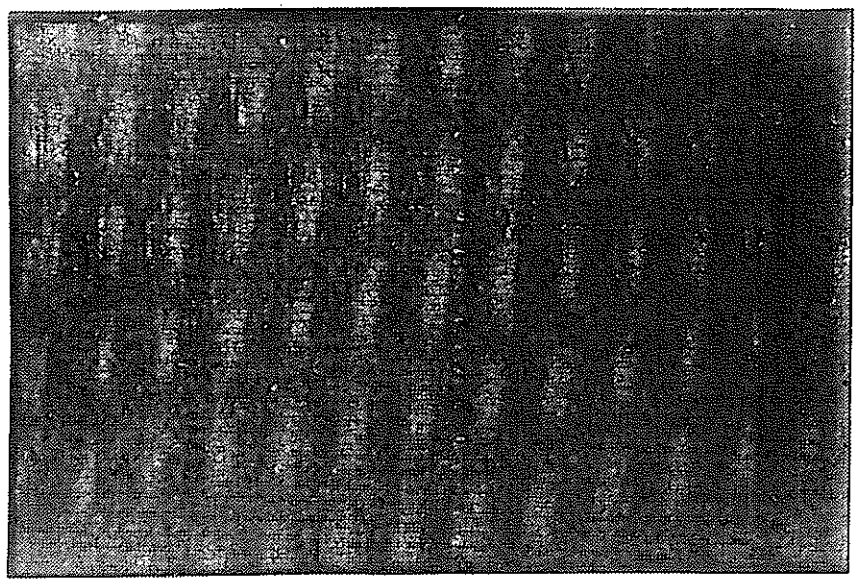

Fig.19 An example of fringe pattern of the moire method for test-piece NDT14 unloaded after tensile testing ($\varepsilon \simeq 3.78\%$)

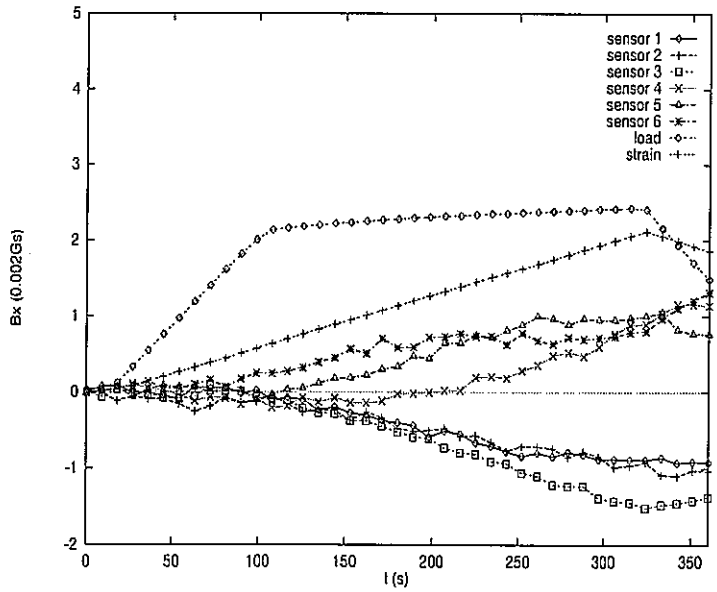

Fig.20 In-Situ signals for test-piece NDT14 and strain range 0.08% ~ 0.5%

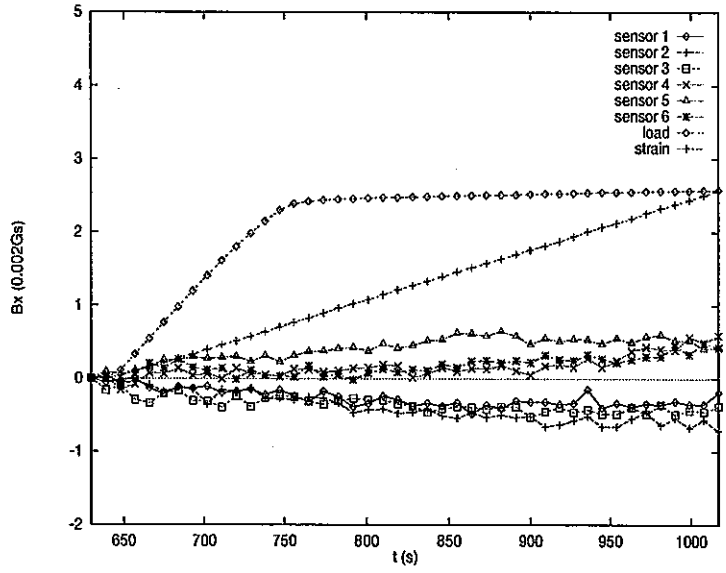

Fig.21 In-Situ signals for test-piece NDT14 and strain range 0.35% ~ 1.08%

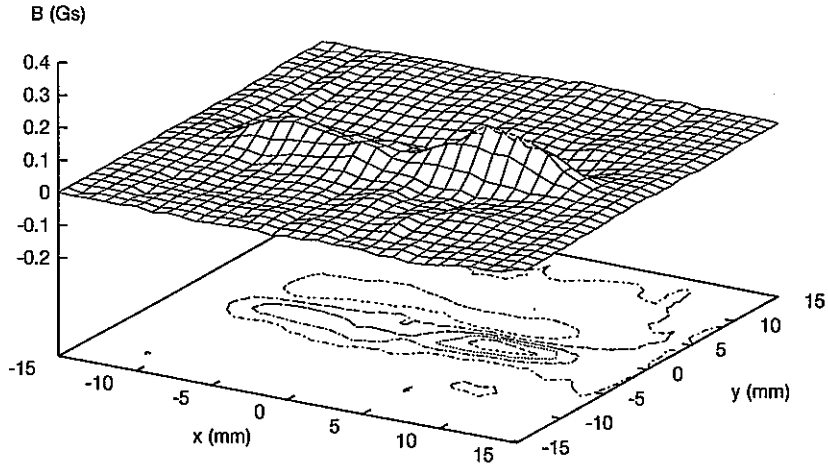

Fig.22 Distribution of the flux density for test-piece NDT21 after fatigue crack was initiated

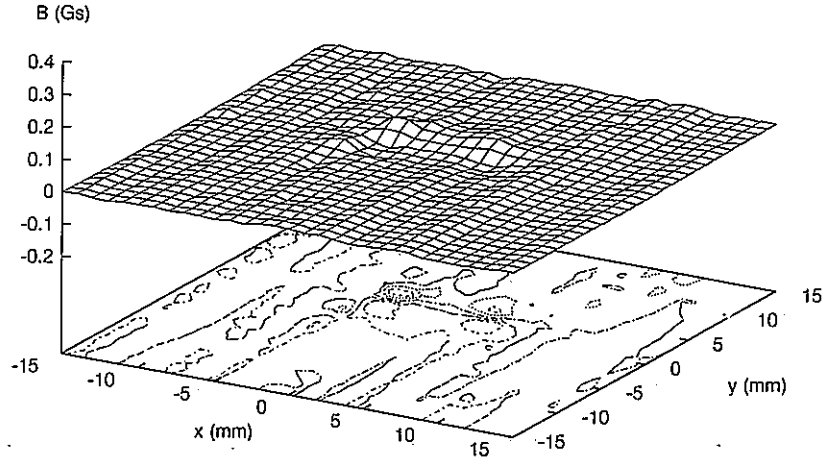

Fig.23 Distribution of the flux density for test-piece NDT20 after fatigue crack was initiated

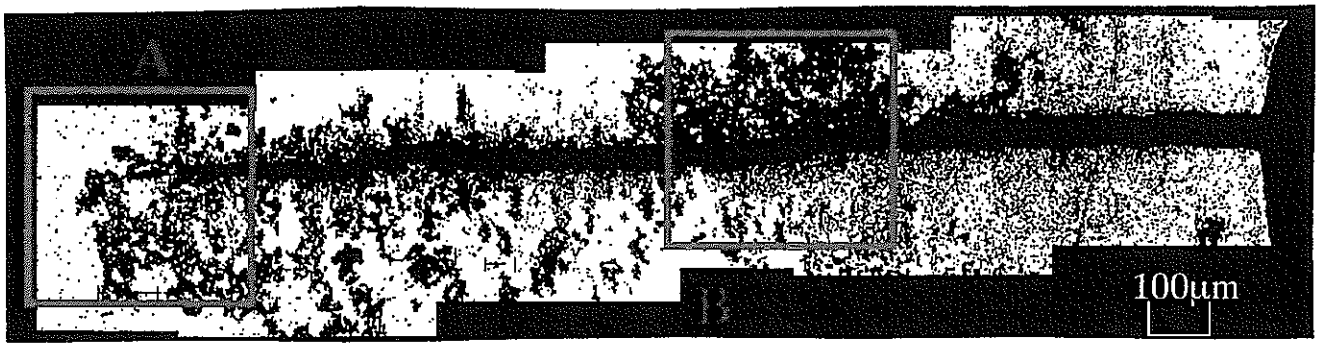

Fig.24 The magnetization image at the crack tip of the test-piece NDT21 obtained by using the colloidal method (Provided by Prof.Y.Nakasone, To be published)

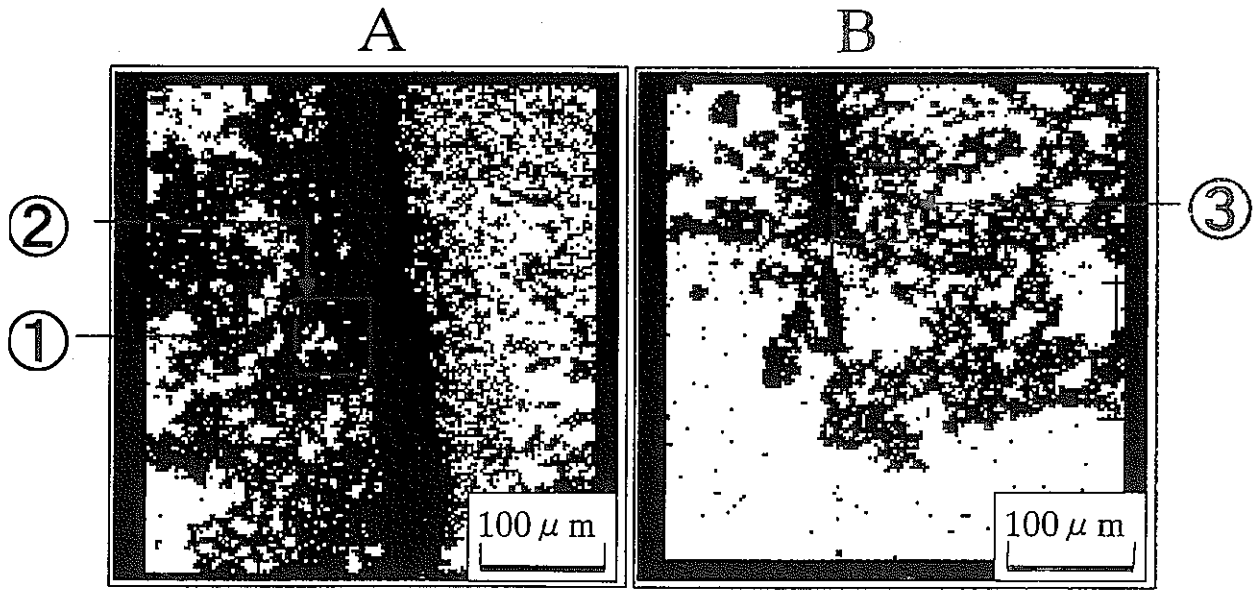

Fig.25 The observing areas of the MFM (Provided by Prof.Y.Nakasone, To be published)

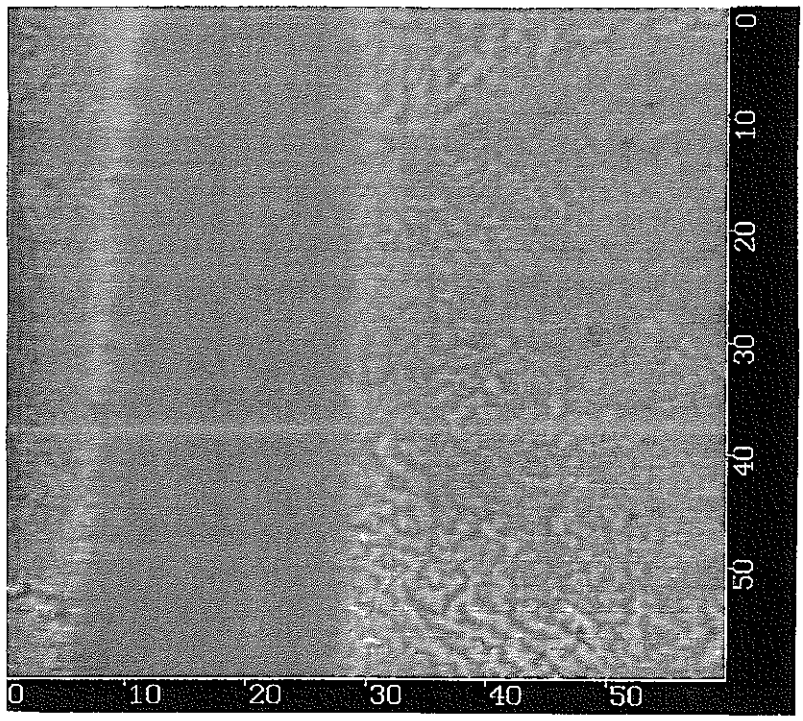

Fig.26 An example of the MFM image at the crack region observed before chemical polishing (Provided by Prof.Y.Nakasone and Dr.T.Suzuki, To be published)

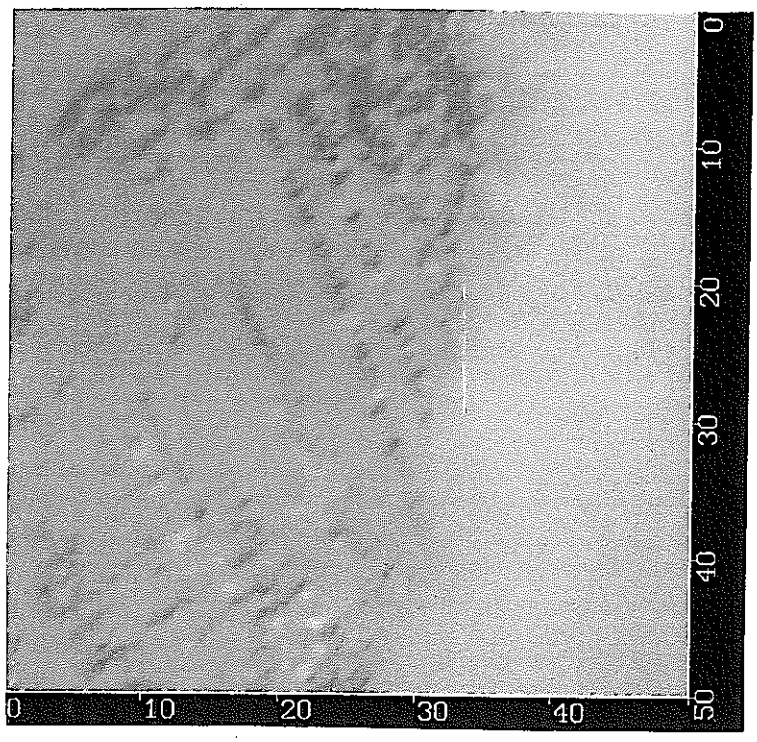

Fig.27 An example of the MFM image at the crack region after chemical polishing
(Provided by Prof.Y.Nakasone and Dr.T.Suzuki, To be published)

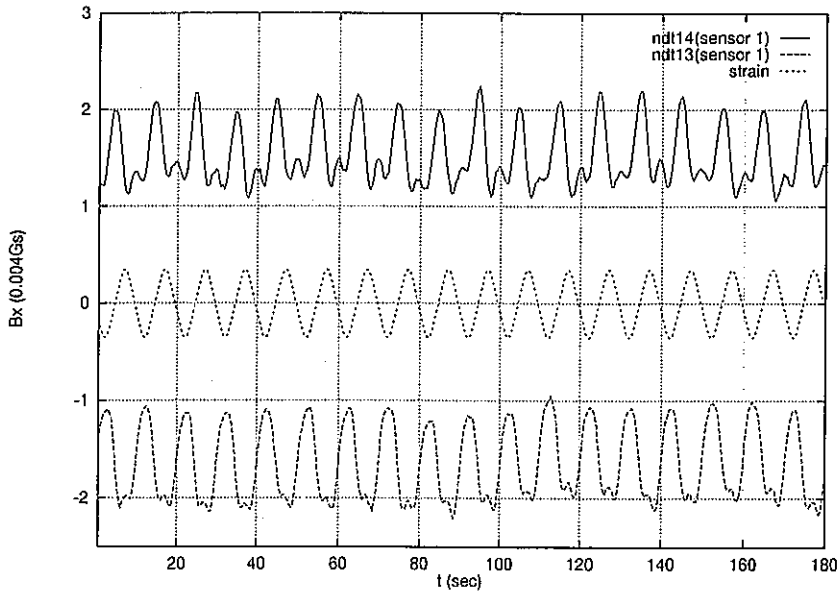

Fig.28 Comparison of magnetic field signal during the fatigue testing of test-piece NDT14
(with residual strain) and NDT13 (virgin material)

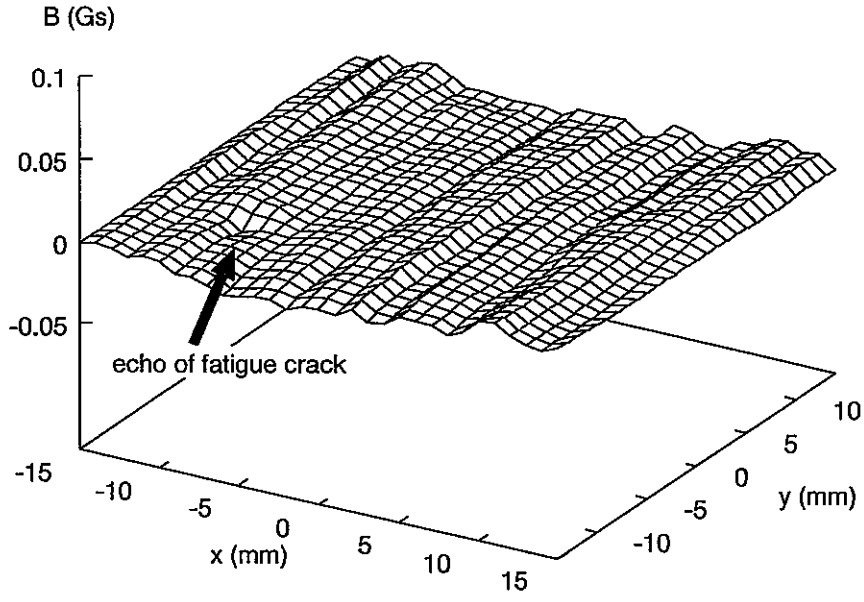

Fig.29 Distribution of magnetic field measured after fatigue crack initiated (NDT13, 63000 cycle)

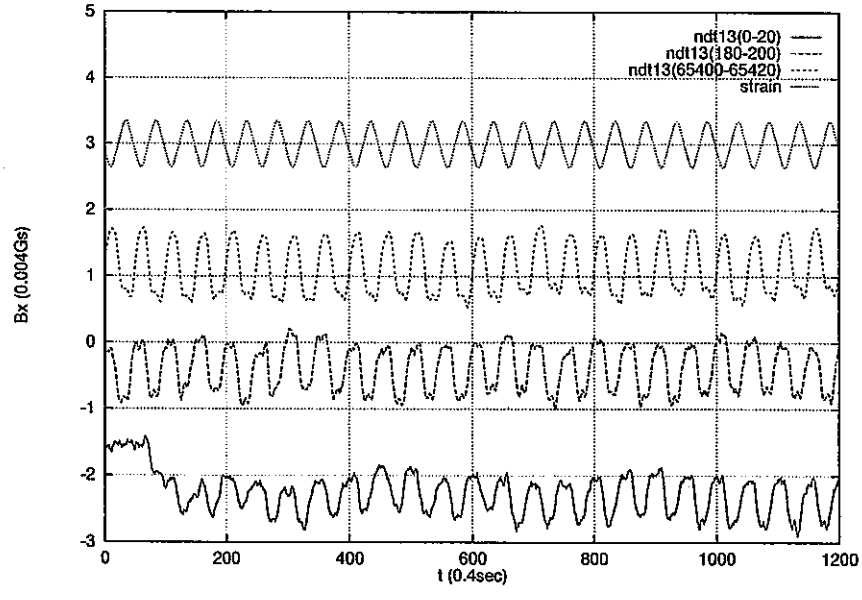

Fig.30 Magnetic field signal at different cyclic number for test-piece NDT13 (virgin material)

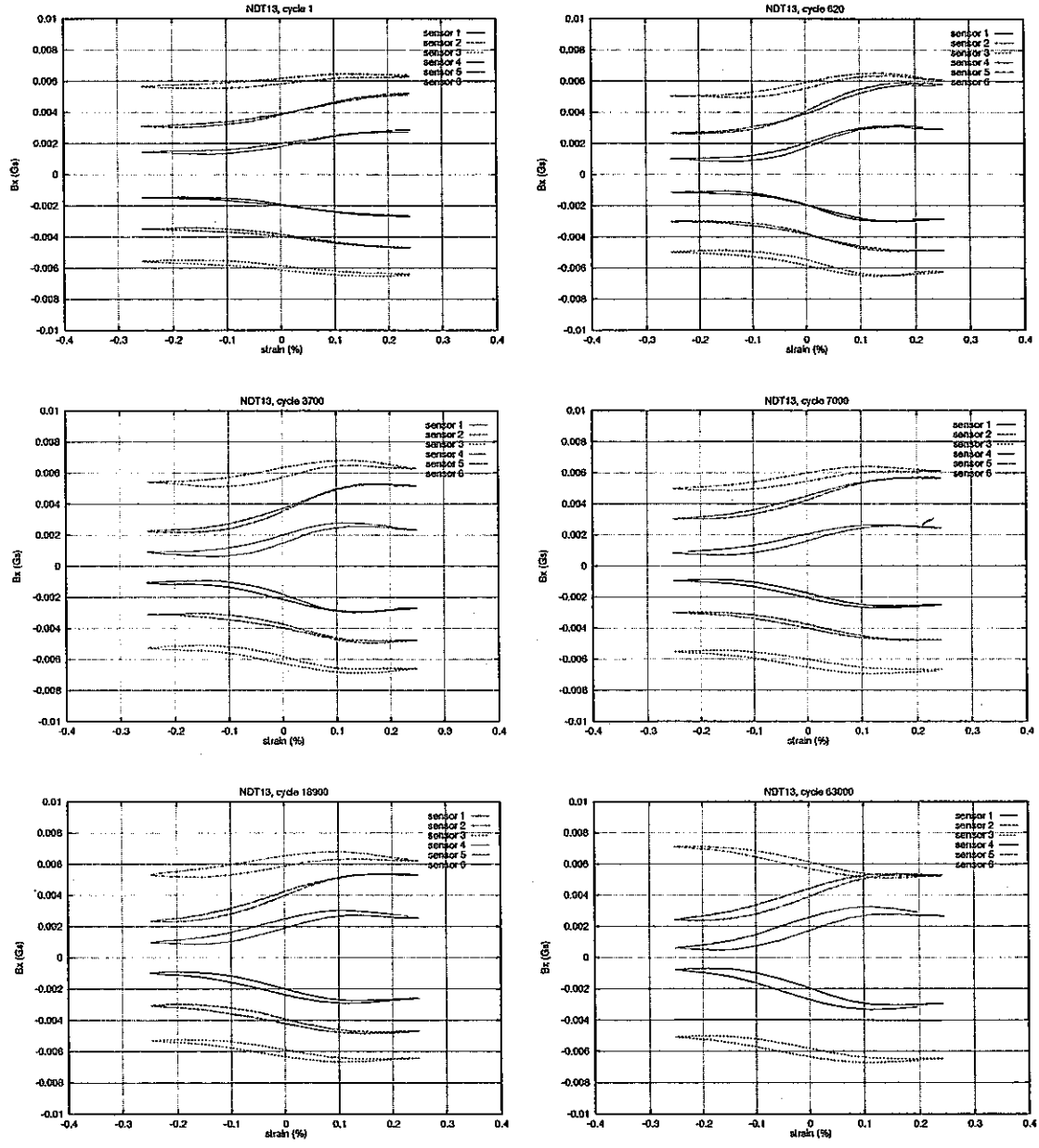

Fig.31 Typical hysteresis curves of the magnetic field versus applied strain

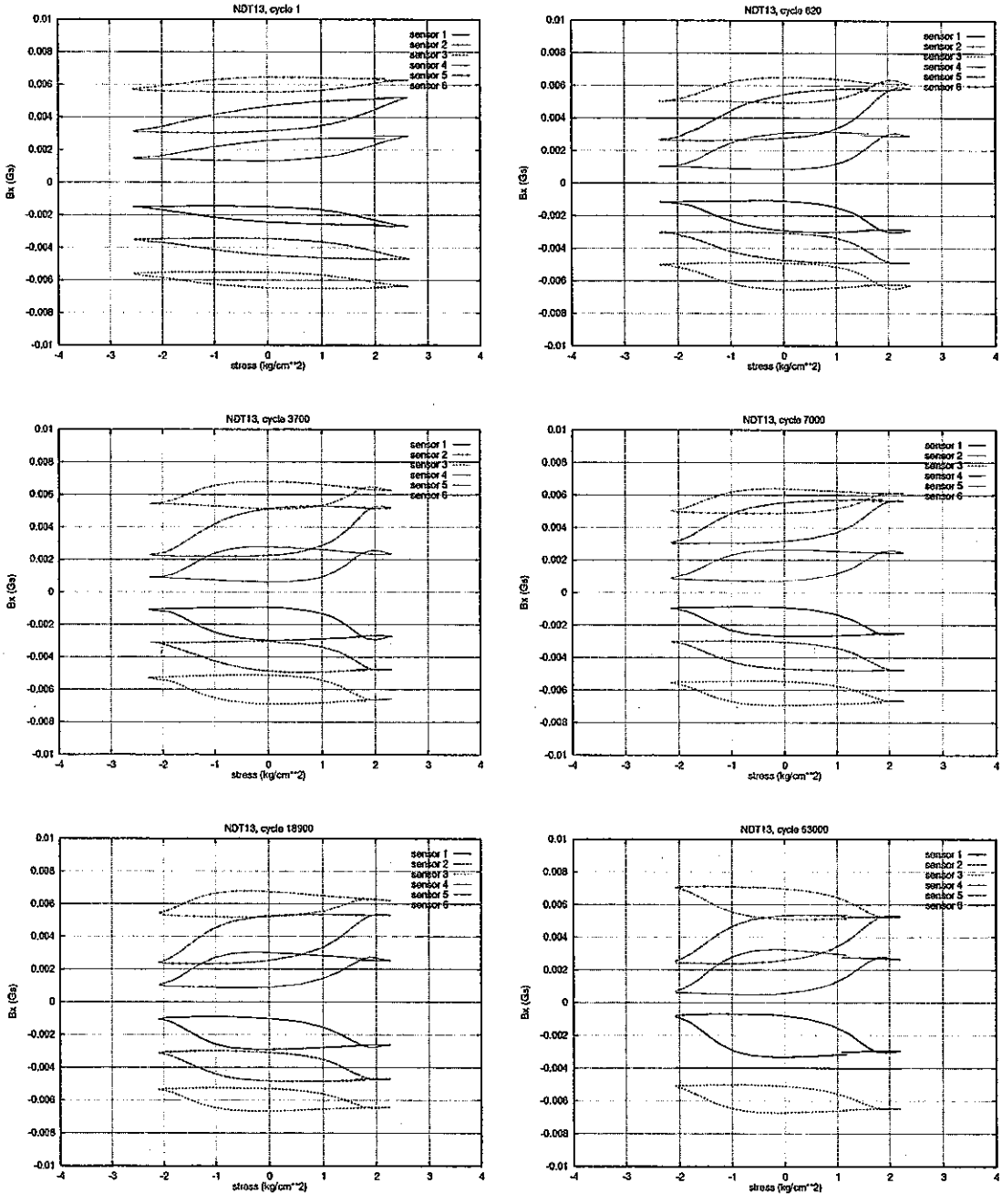

Fig.32 Typical hysteresis curves of the magnetic field versus applied loading

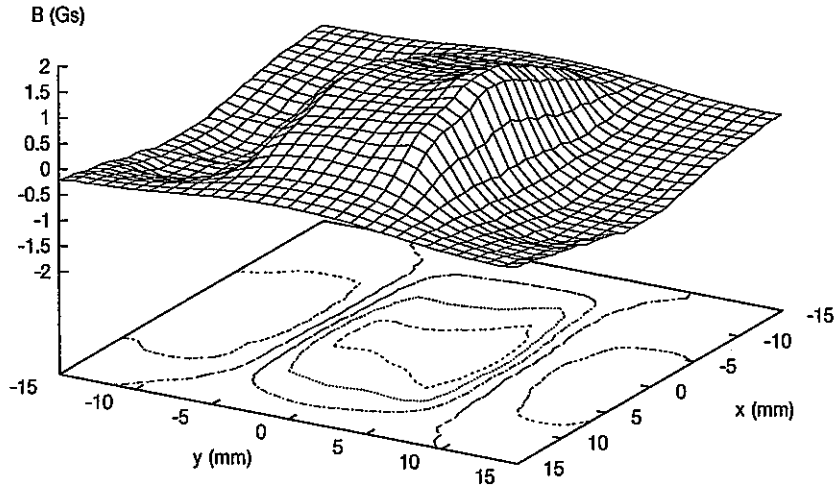

Fig.33 Distribution of the residual magnetic field B_y after magnetized with a permanent magnet (NDT12, Residual strain: 0.84%)

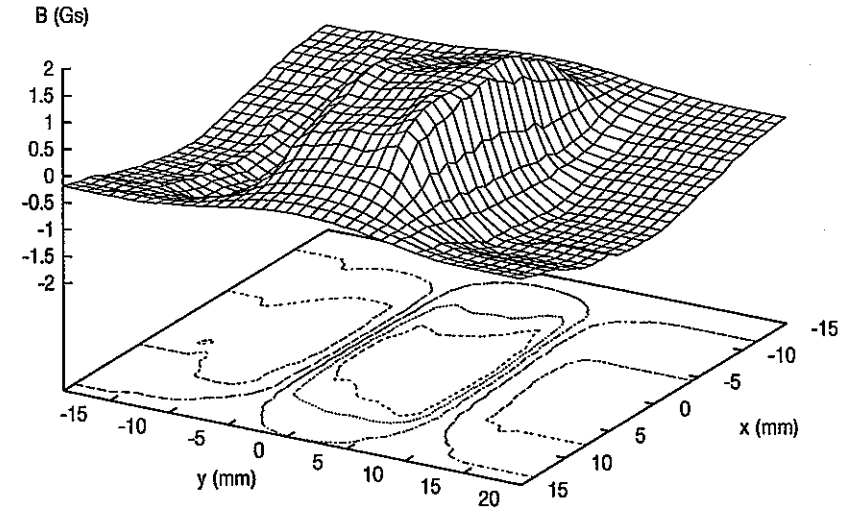

Fig.34 Distribution of the residual magnetic field B_y after magnetized with a permanent magnet (Residual strain: 1.82%)

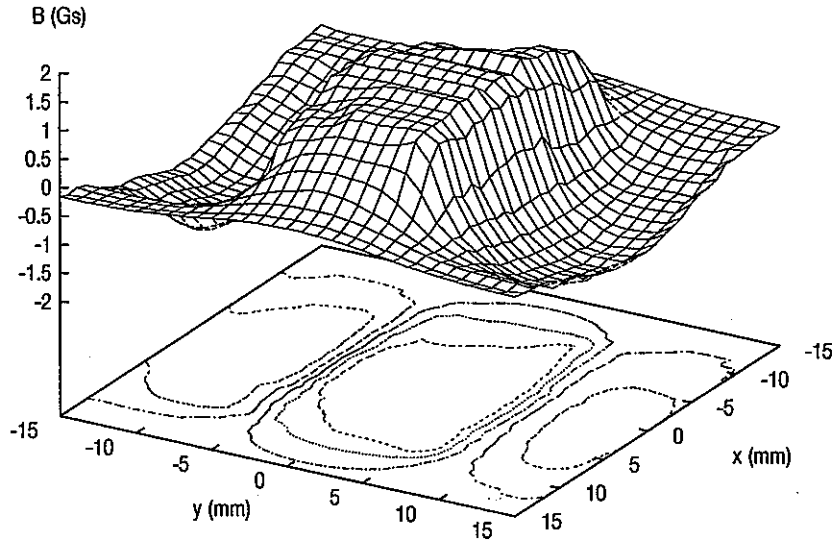

Fig.35 Distribution of the residual magnetic field B_y after magnetized with a permanent magnet (Residual strain: 5.76%)

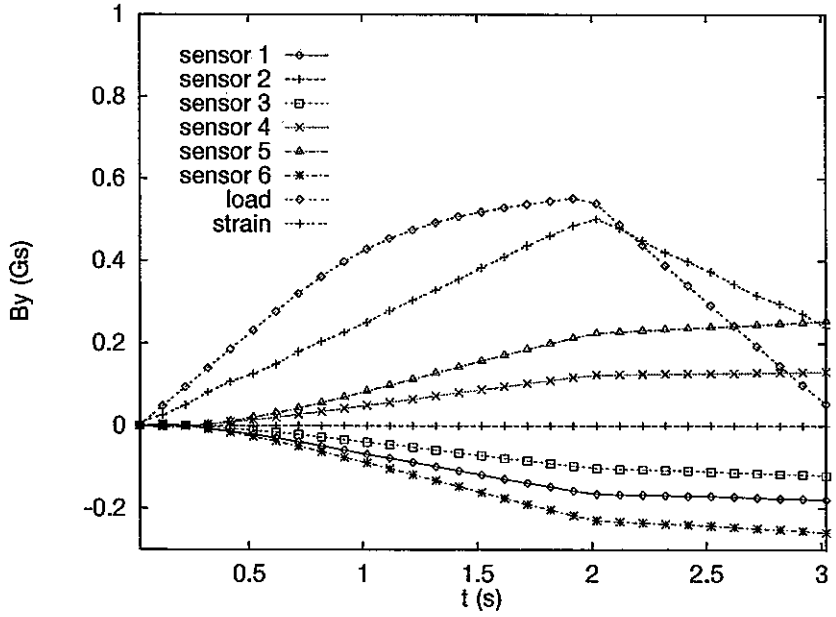

Fig.36 In-Situ measuring result for the magnetized test-piece NDT12 (strain range, $0 \sim 0.2\%$)

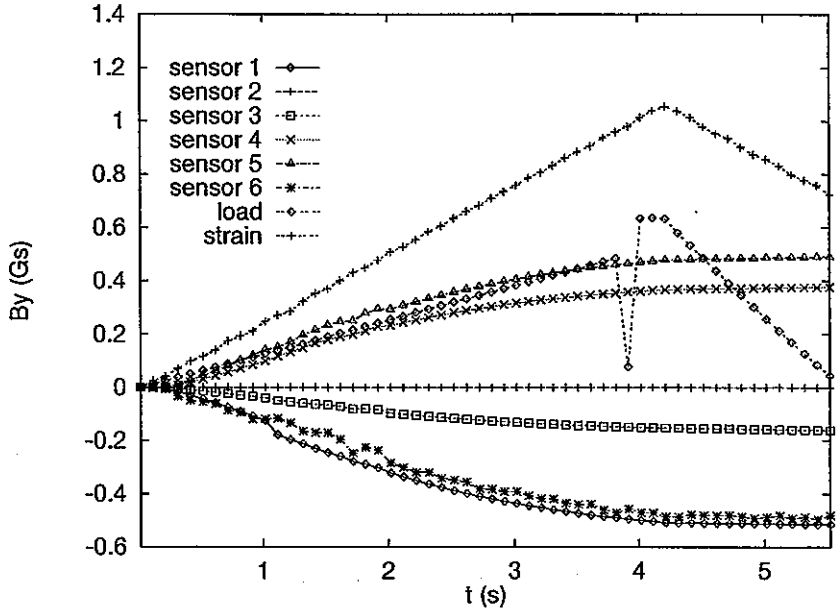

Fig.37 In-Situ measuring result for the magnetized test-piece NDT12
(strain range, 0.08% ~ 0.5%)

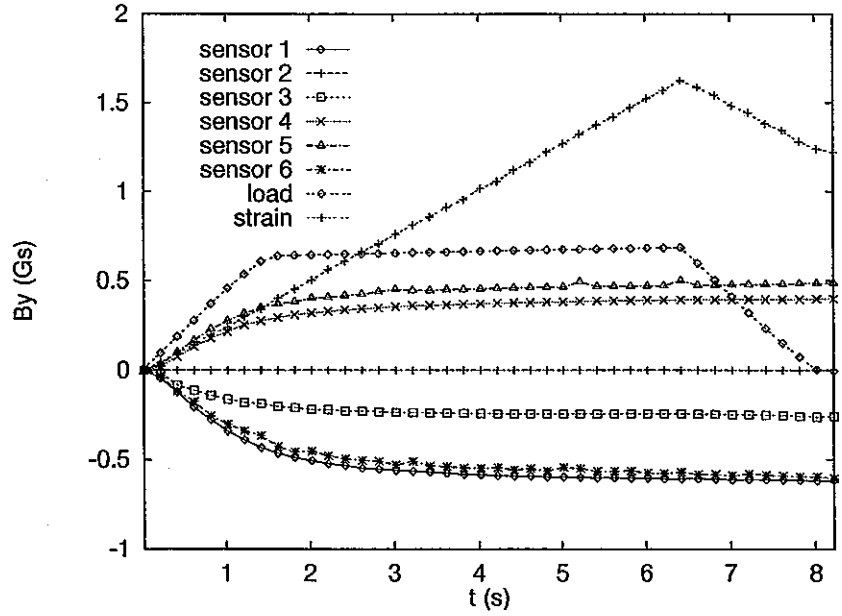

Fig.38 In-situ measuring result for the magnetized test-piece NDT12
(strain range, 0.35% ~ 1.0%)

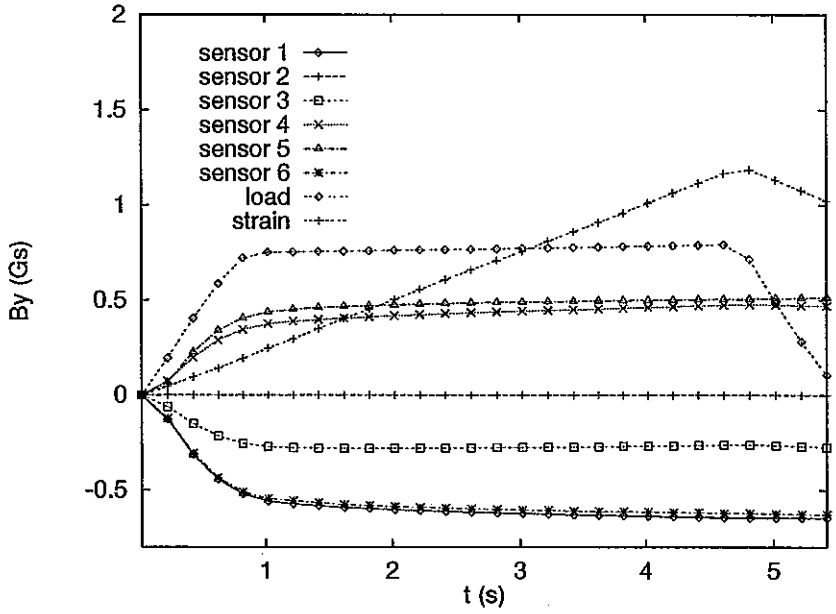

Fig.39 In-situ measuring result for the magnetized test-piece NDT12
(strain range, 0.95% ∼ 2.0%)

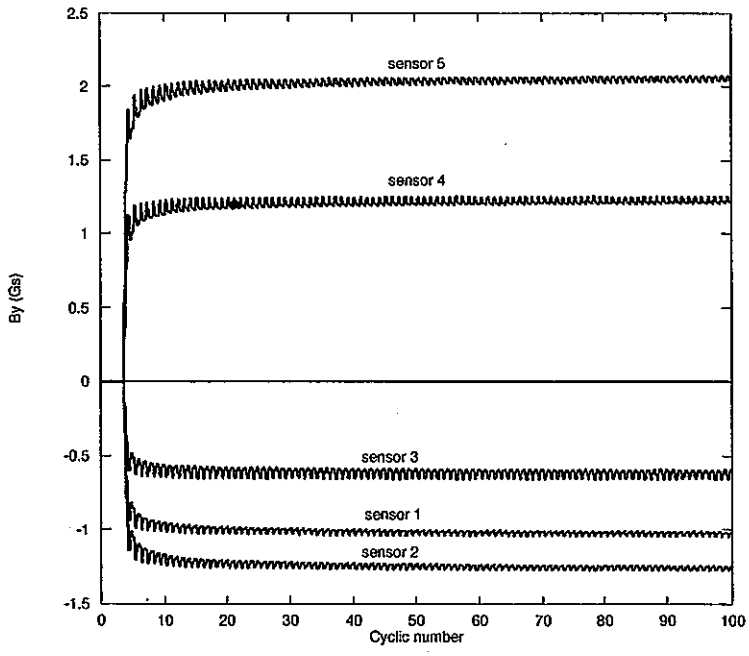

Fig.40 In-Situ signal of the magnetic field for test-piece NDT12, which is demagnetized/magnetized after a tension to a strain of 6.0% (0 ∼ 100 cycle)

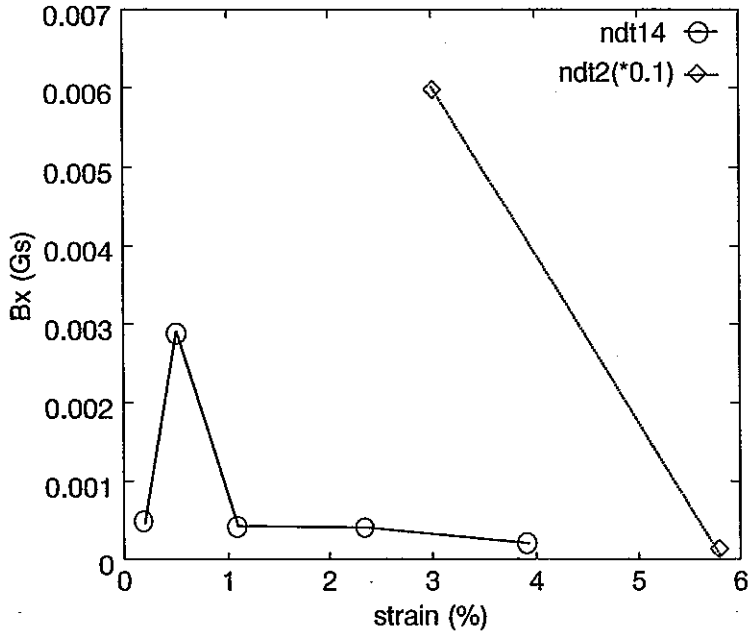

Fig.41 The decrement of the plastic deformation induced magnetization for the test-piece NDT14 and test-piece NDT2

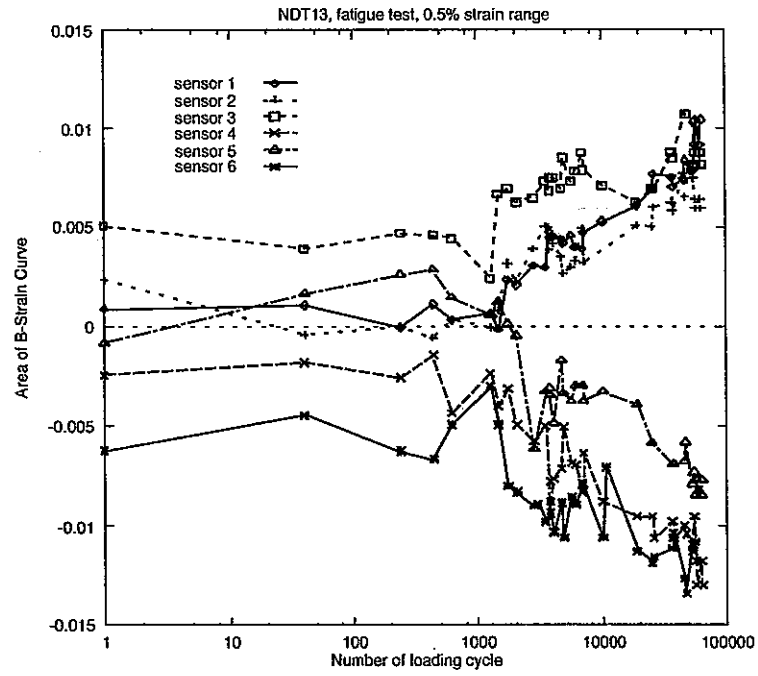

Fig.42 Evolution of the area of the $B-\varepsilon$ hysteresis curve during fatigue testing for test-piece NDT13

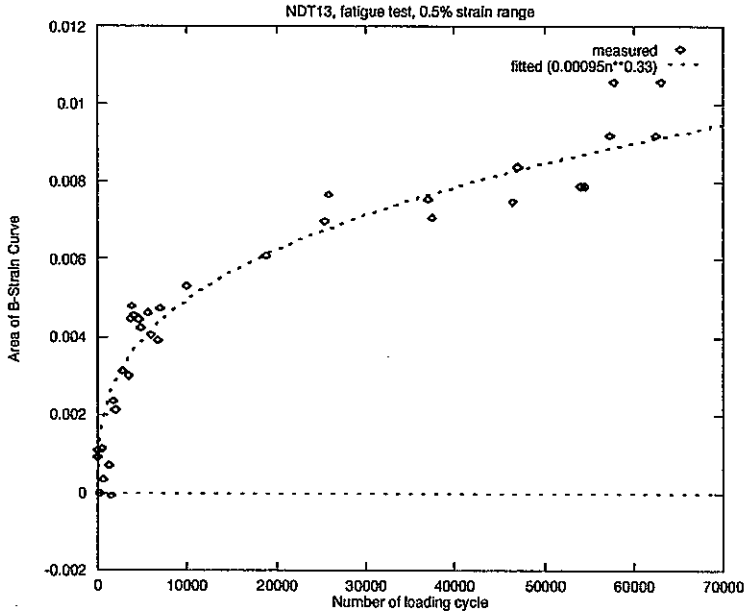

Fig.43 Evolution of the area of the $B - \varepsilon$ hysteresis curve during fatigue testing for test-piece NDT13 and sensor 1

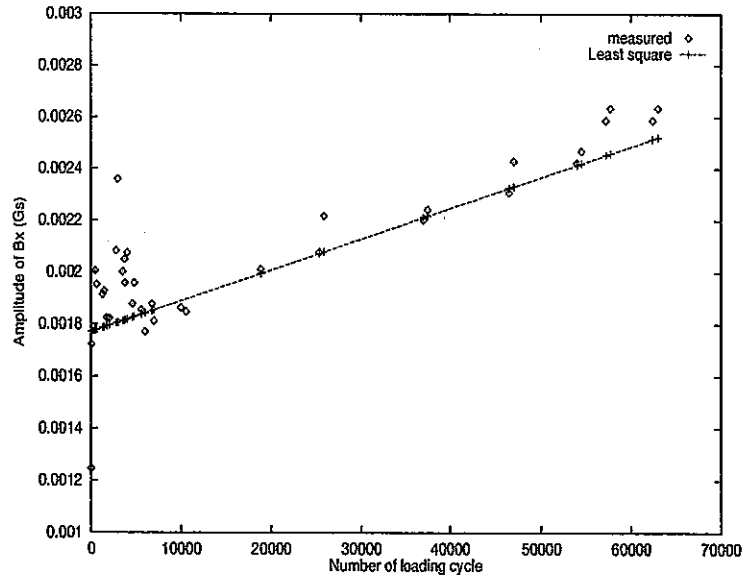

Fig.44 Correlation of the cycle number and the amplitude of the measured natural magnetic field

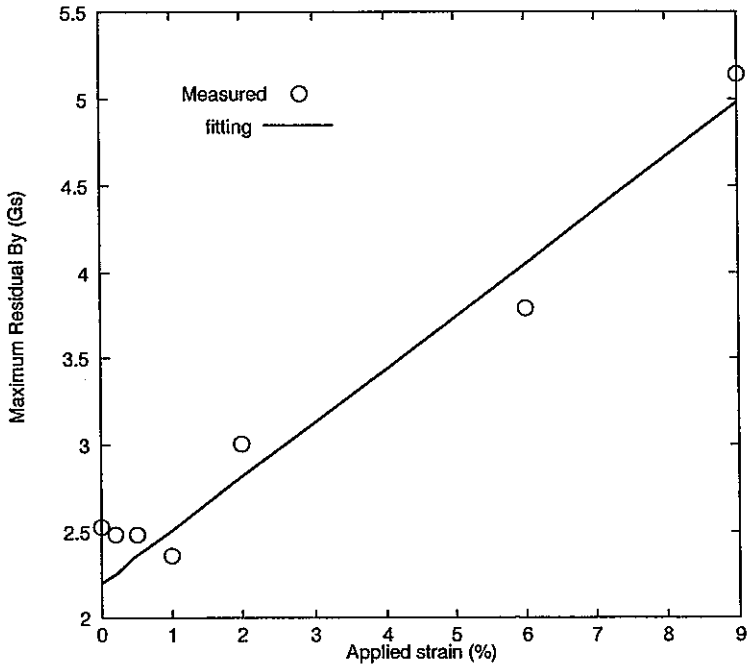

Fig.45 Correlation of the residual magnetic field and the applied plastic strain

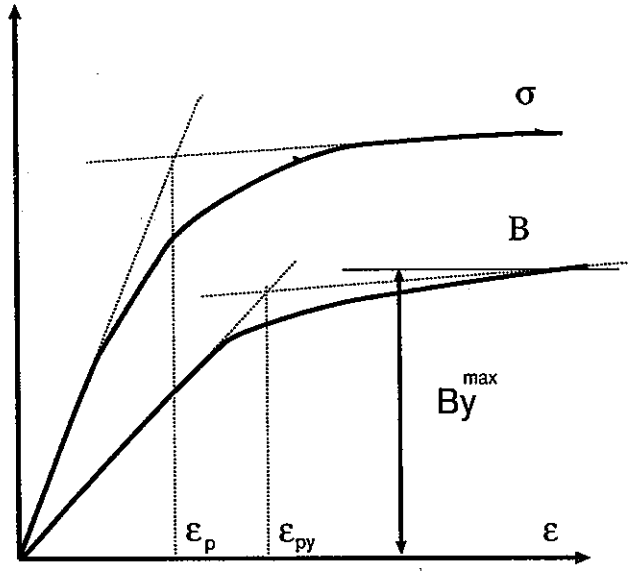

Fig.46 The concept diagram for the definition of the ε_p, ε_{py} and B_y^{max} used in table 5